NOVEL FABRICATION TECHNIQUES AND APPLICATIONS FOR HYDROGENATED AMORPHOUS SILICON

by

Werner Pries

A thesis
presented to the University of Manitoba
in partial fulfillment of the
requirements for the degree of
Master of Science
in
Electrical Engineering

Winnipeg, Manitoba, 1984

(c) Werner Pries, 1984

NOVEL FABRICATION TECHNIQUES AND APPLICATIONS

FOR HYDROGENATED AMORPHOUS SILICON

BY

WERNER PRIES

A thesis submitted to the Faculty of Graduate Studies of
the University of Manitoba in partial fulfillment of the requirements
of the degree of

MASTER OF SCIENCE

© 1984

Permission has been granted to the LIBRARY OF THE UNIVERSITY OF MANITOBA to lend or sell copies of this thesis. to the NATIONAL LIBRARY OF CANADA to microfilm this thesis and to lend or sell copies of the film, and UNIVERSITY MICROFILMS to publish an abstract of this thesis.

The author reserves other publication rights, and neither the thesis nor extensive extracts from it may be printed or otherwise reproduced without the author's written permission.

ABSTRACT

The electrical and optical properties of hydrogenated amorphous silicon, fabricated for the first time by activated reactive evaporation(ARE), have been measured for various partial pressures of hydrogen employed during deposition. Incorporation of both molecular and atomic hydrogen is implied by the behaviour of the dark conductivity, which decreases from approximately 10^{-4} S cm^{-1}, to less than 10^{-8} S cm^{-1} with a corresponding increase in the optical gap from 1.4 to 1.7 eV. The incorporation of atomic hydrogen is appreciably enhanced by increasing the reaction probe voltage. High deposition rates (0.04-0.1 μm/min) and excellent film uniformity make ARE an attractive alternative fabrication technique to conventional radio-frequency glow-discharge deposition, provided the deposition parameters and unwanted impurities can be controlled.

The use of hydrogenated amorphous silicon as an archival storage medium by means of hydrogen exo-diffusion has been demonstrated. Changes in optical reflectivity of hydrogenated amorphous silicon films of up to 90% have been induced by argon laser processing. Accompanying changes by more than 4 orders of magnitude in resistivity also provide a

mechanism for interrogation of the stored data by an electron-beam. Storage densities as high as 10^9 bits/in^2 for optical recording and 10^{11} bits/in^2 for recording with electron beams are predicted on the basis of these results.

A mechanism for in-situ monitoring of hydrogen incorporation into amorphous silicon has been demonstrated. Based on temporal changes in reflectivity during the growth of hydrogenated amorphous silicon films, this mechanism is shown to provide for an accurate determination of the degree of hydrogen incorporation, as well as the growth rate of the growing film. This mechanism is described experimentally and modelled phenomenologically, and is expected to provide a basis for in-situ correlation of hydrogen incorporation with process parameters.

ACKNOWLEDGEMENTS

The author would like to thank his advisor, Prof. H.C. Card, for his encouragement and assistance through the course of this project.

The author also wishes to thank Prof. K.C. Kao for his assistance and helpful discussions. Special thanks are extended to my colleague, R.D. McLeod, with whom I shared a great deal of experimental work and discussions. The author also wishes to thank his colleagues at the Materials and Devices Research Laboratory and at the VLSI Research Laboratory for their assistance and cooperation.

Financial support from the Natural Sciences and Engineering Research Council of Canada is gratefully acknowledged.

CONTENTS

ABSTRACT iv

ACKNOWLEDGEMENTS vi

Chapter page

I. INTRODUCTION 1

Hydrogenated Amorphous Silicon: An Overview . . 2
Amorphous Materials Research at MDRL 5
Organization of this Thesis 7

II. FABRICATION OF A-SI:H THIN FILMS 9

Properties of a-Si:H Deposited by ARE 10
Activated Reactive Evaporation 11
Experimental Techniques 13
Experimental Results 15
Further Results 23

III. HYDROGENATED AMORPHOUS SILICON FOR ARCHIVAL STORAGE 25

Archival Storage Techniques 25
New Storage Methods Using a-Si:H 29
Experimental Techniques 30
Experimental Results 31
Theoretical Evaluation 36
Laser Processing 36
Electron-beam Processing 39
Storage Density Limitations 39
Laser Processing 40
Electron-beam Processing 44
Discussion 46

IV. TECHNIQUES FOR MONITORING FILM FABRICATION 48

In-Situ Monitoring of Hydrogen Incorporation in a-Si:H 49
Experimental Techniques 50
Experimental Results 51
Determination of the Extinction Coefficient 55
Discussion 62

V. CONCLUSIONS 64

Appendix page

A. OPTICAL PROPERTIES OF THIN FILMS 67

REFERENCES 75

LIST OF FIGURES

Figure		page
2.1	Schematic of ARE deposition system	15
2.2	Deposition rate (μm/min) vs. H_2 partial pressure.	17
2.3	Conductivity and activation energy vs. H_2 partial pressure	18
2.4	Refractive index vs. H_2 partial pressure	21
2.5	Optical gap vs. H_2 partial pressure	22
3.1	Writing Mechanisms for Storage Systems	27
3.2	Reflectivity vs. Ar Laser Power	32
3.3	Reflectivity and conductivity vs atomic H content.	34
3.4	Refractive index and extinction coeff. vs. atomic H content.	35
3.5	Reflectivity vs. thickness.	38
3.6	Temperature profile for laser annealing	43
4.1	Reflection Coefficient vs. Film Thickness	53
4.2	Experimental Reflection vs. Film Thickness.	54
4.3	Inverse Error of Reflection and Transmission Coefficients.	58
4.4	Peaks in Reflectivity as a Function of n and d	59
4.5	Upper Envelope of Reflection Curve	61
4.6	Envelope Decay β as a Function of α	61
4.7	Absorption Coefficient (α) vs Hydrogen Content	63
A.1	Thin Film Reflection and Transmission Models	68

A.2 Frontside Reflection Coefficient 73

A.3 Backside Reflection Coefficient 74

Chapter I

INTRODUCTION

Empirical research in amorphous semiconductors has progressed as a natural extension to the work performed on crystalline semiconductors. However, due to the random nature of amorphous materials, the understanding of the basic physics has progressed rather slowly. Although the history of amorphous materials research dates back nearly 50 years, it has only been in the last 10 years that interest in these materials and particularly in amorphous silicon (a-Si) has accelerated. This is evidenced by the number of papers published in the area of amorphous silicon: pre-1970, 94 ; 1970-1979, 1229; 1980-1982, 1383.

Although the primary methods of fabrication are by the glow-discharge technique, it is in the pursuit of alternate techniques for the fabrication of high-quality hydrogenated amorphous silicon (a-Si:H) that the activated reactive evaporation (ARE) method has been developed [1]. Other developments presented in this thesis are new techniques for the application of a-Si:H for archival storage devices [2,3] and a novel method of in-situ film-growth monitoring for use in process optimization and control [4,3].

1.1 HYDROGENATED AMORPHOUS SILICON: AN OVERVIEW

Amorphous silicon (a-Si) is characterized by a short range ordering of up to the third or fourth nearest neighbor atoms whereas long range ordering is not maintained. It is due to the short range ordering that the a-Si exhibits many characteristics common to crystalline silicon (c-Si). Pure a-Si is permeated by dangling bonds with a concentration on the order of 10^{19} cm^{-3}. The dangling bonds produce states within the energy gap and contribute to electrical conduction and optical absorption processes. Further, these states often act as carrier traps or recombination centers and thereby reduce the mobility or carrier lifetimes. In addition, the large density of states makes it difficult to affect the energy of the Fermi level, effectively eliminating doping capabilities.

The first report on the incorporation of hydrogen into the a-Si network was by Chittick et. al. in 1969 [5] and was performed by glow-discharge deposition. This was significant for two reasons. Firstly, all previous work in a-Si was hampered by the high density of states due to dangling bonds, resulting in an undopable material, unsuitable for semiconductor applications. These materials were shown to have a very low dark conductivity ($\sigma_d < 10^{-10}$ S cm^{-1}) and a significant photoconductivity. It was not immediatly known why this material had these qualities until it was shown by

the field effect method [6,7] that hydrogen reduced the density of states within the energy gap. Subsequent thermal annealing studies confirmed these results. Secondly, the report by Chittick was the first to demonstrate the use of the glow-discharge technique in a constructive manner for a-Si fabrication. In fact, until 1976, very little research was performed with respect to glow-discharge systems. The resulting materials are defined as hydrogenated amorphous silicon (a-Si:H) which in some cases contain up to 35% atomic hydrogen.

Spear and LeComber in 1975 [8] and 1976 [9] reported the first successful attempts at substitutional doping using diborane and phosphine. This success in doping directly affected the success of applications-oriented research. As a result, the first p-n junctions [10] and photovoltaic devices [11] were reported in 1976. Although the primary thrust of applications research has been towards the development of photovoltaic devices, many other applications have been and are being developed. These include Schottky barrier devices in 1976 [12], image sensor ICs in 1980 [13] and charge coupled devices (CCD) in 1982 [14].

The a-Si:H research can be divided into four main categories. These are characterization, fabrication, applications, and basic physics. Many of the characterization techniques have been adopted from those developed for c-Si

research and as a result this is not a particularly active area. The amount of research concerned with the development of fabrication techniques is still fairly significant. Prior to 1970, most fabrication was performed by electron-beam evaporation without the incorporation of hydrogen. However, since the early 1970s, much work has been performed on the use and understanding of the glow-discharge and sputtering techniques. Work with chemical vapor deposition (CVD) systems has been an area of interest since 1978. Recently, several groups have returned to the electron-beam evaporation technique with the purpose of incorporating atomic hydrogen during or following film deposition by hydrogen plasma techniques or ion implantation.

As already stated, the study of applications has followed the successful demonstration of substitutional doping and as a result has flourished since 1977. It is the ability to produce large-area depositions at low cost which makes a-Si:H a targeted material for photovoltaic purposes. However, for the same reason, this material has been found to be suitable for thin film transistors, xerography, CCDs, image sensors, and as an archival storage medium.

Research into the physical properties of a-Si:H has been slow in its development. Due to the random nature of the material, modeling of physical phenomena has proved difficult. However, this has been a very active research area

over the last 7 years. Present research areas include theoretical modeling, structural measurement techniques (electron spin resonance (ESR), infrared (IR), Raman/X-ray, nuclear magnetic resonance (NMR), secondary ion-mass spectrometry (SIMS), Auger, Photoemission, deep level transient spectroscopy (DLTS), field effect transistor (FET), etc.), transport phenomena (conductivity, time-of-flight, thermopower, etc.), photoresponse (absorption, photoluminescence, photoconductivity, Staebler-Wronski effect) and other studies (thermal annealing, interface states, recombination, etc.).

It is apparent that a-Si:H will gain significant status as a new electronic and optical material for many applications. It is expected that in the near future, the volume of a-Si:H solar cells will be surpassed by other applications.

1.2 AMORPHOUS MATERIALS RESEARCH AT MDRL

The Materials and Devices Research Laboratory (MDRL) at the University of Manitoba has been active over the past few years in developing a research program on amorphous materials. The primary areas of study have been in fabrication, materials (amorphous semiconductor alloys), and applications.

Microwave sputtering techniques to fabricate a-Se [15,16] and microwave glow-discharge systems for a-Si:H deposition [17,18] have been developed within our laboratory. Recently, a method of activated reactive evaporation (ARE) for a-Si:H deposition has also been developed [1].

Amorphous Si:Ge alloys have been characterized for their use in photovoltaic applications [19,20]. With the collaboration of several Japanese researchers, a-SiN_x:H alloys have also been characterized [21,22]. As mentioned above, the development in our laboratory of a-Si:H as an archival storage medium has been reported [2,3], as has been the development of an in-situ film growth monitoring technique for the determination of dynamic atomic hydrogen incorporation and film thickness [4,3].

Present research is many faceted. Continuing work includes the microwave glow-discharge system development for a-Si:H fabrication, a-Si:H based archival storage media, and activated reactive evaporation with the incorporation of other elements such as nitrogen. In parallel with the ARE deposition technique is the study of hydrogen-ion implanted a-Si with the cooperation of the Department of Physics, University of Manitoba. Of particular recent interest is the development of a laser-driven chemical-vapor deposition (CVD) system for VLSI interconnection technology based on programmable wire depositions [23].

1.3 ORGANIZATION OF THIS THESIS

This thesis has begun with a general introduction to amorphous semiconductors and to amorphous silicon in particular. An overview of present research in the area of amorphous silicon was followed by a description of the amorphous semiconductor research within the Materials and Devices Research Laboratory (MDRL) at the University of Manitoba.

Chapter 2 reviews thin-film amorphous silicon fabrication techniques including a novel fabrication technique. This technique, developed at MDRL, consists of plasma-activated reactive evaporation of a silicon source in a hydrogen environment to produce hydrogenated amorphous silicon.

Chapter 3 describes our introduction of a-Si:H as a high density archival storage medium using a new approach to data storage. This chapter also includes a description of present storage techniques now used in optical storage systems.

Chapter 4 reviews process control and monitoring techniques in the fabrication of a-Si:H thin films and describes an in-situ monitoring method to determine film thickness and quality. Film quality refers to the degree of atomic hydrogen incorporation, necessary for the passivation of dangling bonds.

Finally, Chapter 5 reviews the results of this work and provides conclusions and recommendations for future work in amorphous silicon-based materials and devices.

Chapter II

FABRICATION OF A-SI:H THIN FILMS

In recent years, efforts have been made to produce a-Si:H films with a sufficiently low density of bandgap states such that their conductivity can be controlled over a wide range by chemical doping. Efforts by Madan [7], Okamoto[24], Taniguchi [25], Dias [26] and others have demonstrated the importance of the deposition conditions with respect to the resultant electrical and optical properties of the films. Their results have shown that given the proper deposition conditions, it is possible to obtain a-Si:H alloys with a low density of bandgap states, high photoconductivity and well defined conduction paths.

The most important deposition methods are glow-discharge deposition (direct current, radio frequency, microwave), sputtering, chemical vapor deposition, and vacuum evaporation. For detailed descriptions of these and other fabrication processes, the reader is referred to Refs. [27,28,29].

2.1 PROPERTIES OF A-SI:H DEPOSITED BY ARE

Electron-beam evaporation is inherently an attractive deposition technique due to its high deposition rate, film thickness uniformity and flexibility in incorporating other elements by co-evaporation. However, evaporation also has several important limitations including lack of control over unwanted impurities and the difficulty of atomic hydrogen incorporation.

Evaporated amorphous silicon is characterized by a large dangling bond density and a correspondingly high ESR spin density [30]. These films are unsuitable for device applications as compared to glow-discharge prepared films. The presence of hydrogen improves the optical and electrical properties of the material by the reduction of the defect state density due to dangling bond termination.

Due to the low cost and high deposition rate common to evaporation systems, it is desirable to produce a-Si:H films with a low density of bandgap states by this method. Recently, several investigators have begun to explore techniques by which hydrogen can be incorporated into evaporated a-Si films. These techniques have included in-situ and post-fabrication processes. Kubler et. al. [30,31] have studied evaporation in an NH_3 ambient with an attempt to incorporate both hydrogen and nitrogen. Others [32,33] have used hydrogen-ion guns directed at the growing film. Some

results by this method indicate a dark conductivity $<10^{-10}$ S cm^{-1}. Post fabrication H incorporation has been performed by either ion implantation or ion diffusion. Ion implantation [34] has developed in some areas due to the use of ion implanters for doping. The method of ion diffusion [35,36] is rather new and therefore has not been fully exploited. These studies have had limited success and much work must still be performed on the development and optimization of evaporated a-Si:H fabrication.

An alternative evaporation method is proposed in an attempt to overcome these difficulties. This method consists of activated reactive evaporation (ARE). Activated reactive evaporation has been used previously for the incorporation of C in TiC [37], O in Al_2O_3 [38] and N in TiN_x [39] deposits. No previous reports in the literature indicate the use of ARE for the incorporation of H in a-Si:H. The techniques and results presented in this chapter indicate that ARE reduces the difficulties associated with conventional Si evaporation systems and qualitatively demonstrates the capability of incorporating molecular or atomic hydrogen.

2.1.1 Activated Reactive Evaporation

The reactive evaporation process consists of evaporating a material in the presence of a reactant gas. In the

present study, the evaporant is high purity silicon and the reactant gas is hydrogen. The reaction between the silicon and the hydrogen reactant gas can take place at the substrate, in the vapor region or on the evaporant surface. Only the first two reaction sites are considered useful since the temperature at the evaporant surface will prohibit an efficient process. In any of these cases, three factors are considered: (a) an adequate supply of reactants, (b) collision between the reactant species, and (c) reaction between the colliding species [38].

The mean-free path of the reactant species is inversely proportional to the hydrogen partial pressure and to the source-substrate distance. Therefore, if the source-substrate distance is shorter than the mean free path, reactions can take place at the substrate only. On the other hand, if the partial pressure is high, reactions will be possible in the vapor phase also and with sufficient reactants available, high deposition rates are possible. Therefore, for high deposition rates, vapor phase reactions are necessary.

Although collisions of reactant species is necessary, it is not sufficient. The efficiency of a collision is determined by the probability that a reaction has occurred. Factors influencing this efficiency include the chemical nature of the species, stability of the reactant gas, the

free energy of formation of the compound, the dissociation pressure and temperature of the compound, the substrate temperature, etc. [38]. The efficiency of the collisions can be enhanced by activating one of the reactants. This is often necessary when high deposition rates are required. This explains the process being referred to as activated reactive evaporation.

2.1.2 Experimental Techniques

Electron-beam evaporation of silicon was performed in a vacuum system which consisted of a diffusion pump and a cryogenic trap. Metal seals were used except for the work chamber which was a glass bell jar sealed by viton L-gaskets and several electrical and mechanical feed-throughs sealed by viton O-rings. This system had a low ultimate pressure ($\cong 2 \times 10^{-7}$ torr), a high pumping speed and demonstrated convenience of operation. The main disadvantage was the 200°C temperature limit to which the bell jar could be pre-baked.

High-purity polycrystalline silicon was used as the evaporant. The silicon was heated in a steel crucible by electron bombardment. The subtrates employed were soda glass, quartz or crystalline silicon. The substrate temperature was controlled by a filament heater, maintained such that the entire chamber was at equilibrium during deposition. The source-substrate distance was 10 inches.

The silicon source was heated from an electron-beam source in a hydrogen partial pressure of 10^{-4} to 10^{-3} torr. To enhance the atomic hydrogen incorporation, an electrode was placed in the reaction zone as shown in Fig. 2.1. The probe, held at a positive potential (0-500V), draws primary and secondary electrons into the reaction zone, ionizing and activating the reaction gas. It is also believed that a process similar to corona discharge enhances the ionization.

For the results presented in this chapter, the following deposition conditions were employed:

e-beam current: 200 mA at 4000V potential
base pressure: 4×10^{-7} torr
probe voltage: 0 or 200V
hydrogen partial pressure: 10^{-4}-10^{-3} torr
substrate temperature: 200°C

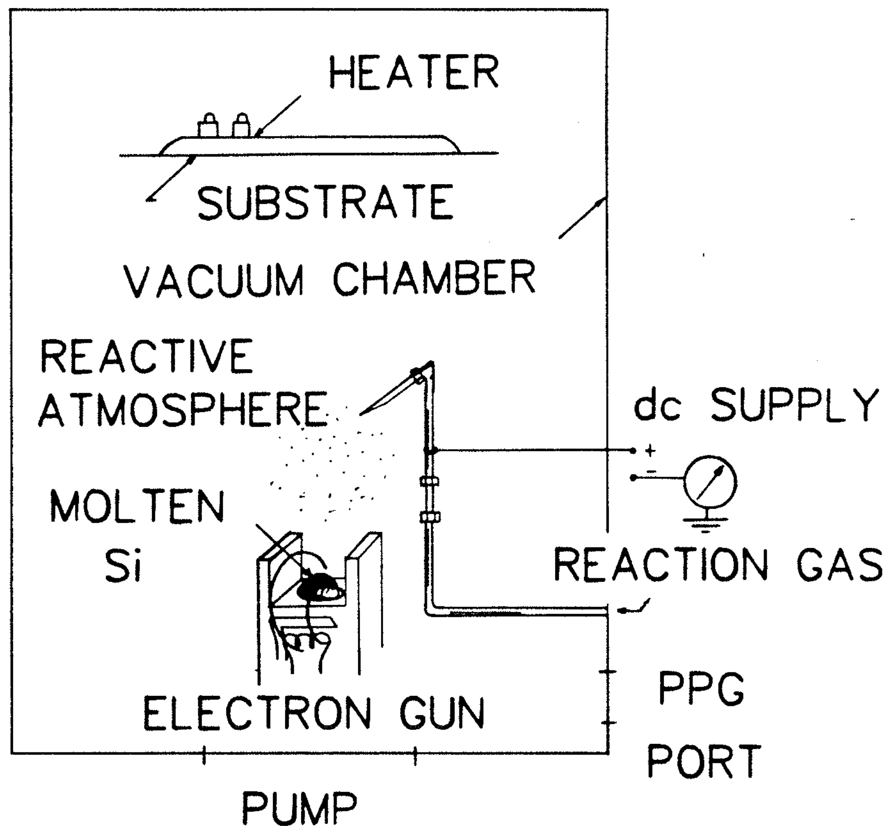

Figure 2.1: Schematic of ARE deposition system

2.1.3 Experimental Results

Methods used for film characterization included scanning electron microscopy with X-ray microanalysis, infrared and visible spectrophotometry, ellipsometry, temperature-dependence of conductivity, photoconductivity, Raman spectroscopy and thermal annealing techniques.

Figure 2.2 illustrates the dependence of the deposition rate upon the hydrogen partial pressure. The deposition rate was found to be invariant to the probe voltage. The variation in the deposition rate at a given partial pressure of H_2 has been attributed to the properties and size of the melt, and to the variations in thermal conductivity at the interface between the melt and the crucible. Excellent film uniformity was obtained when a 10 inch separation was maintained between melt and substrate as evidenced by spectrophotometry results. This was corroborated by a well-defined extinction in ellipsometry measurements.

Figure 2.3 shows the typical dependence of the dark conductivity and the extended-state activation energy of the a-Si:H films upon the partial pressure of H_2, for samples prepared at probe potentials of 0 and 200 V. Intermediate results are obtained at lower probe voltages. The dark conductivity and activation energy associated with the ARE fabrication process at a partial pressure of $H_2 = 6 \times 10^{-4}$ torr are comparable to r.f. glow-discharge produced films. This correspondence provides evidence of effective activation of the reactant gas with subsequent incorporation of atomic hydrogen in the growing film. A similar correspondence has been demonstrated between ARE-fabricated films and H ion implantation of e-beam evaporated films.

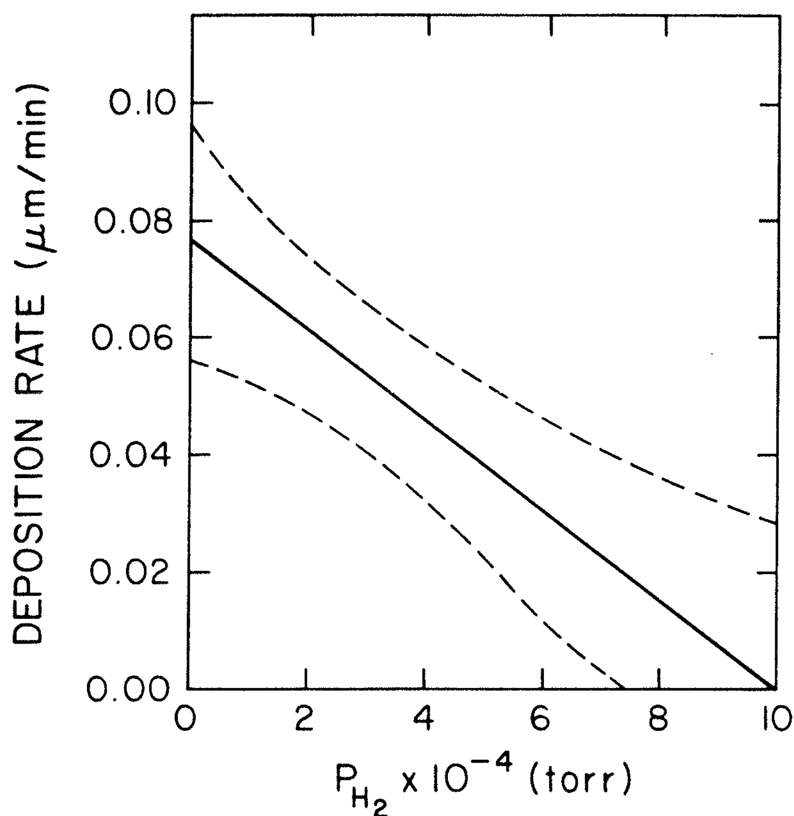

Figure 2.2: Deposition rate (μm/min) vs. H_2 partial pressure. Dashed lines represent the 90% confidence interval.

Although the results are not shown here, a significant reduction was observed in the photoconductivity as compared to r.f. glow-discharge films. Investigations of the absorption bands at 640 cm^{-1} and 1050 cm^{-1} by IR spectroscopy indicate that significant oxygen is incorporated into the films when the H partial pressure is high. The degree of O incorporation is observed to increase as the partial pressure of H_2 increases.

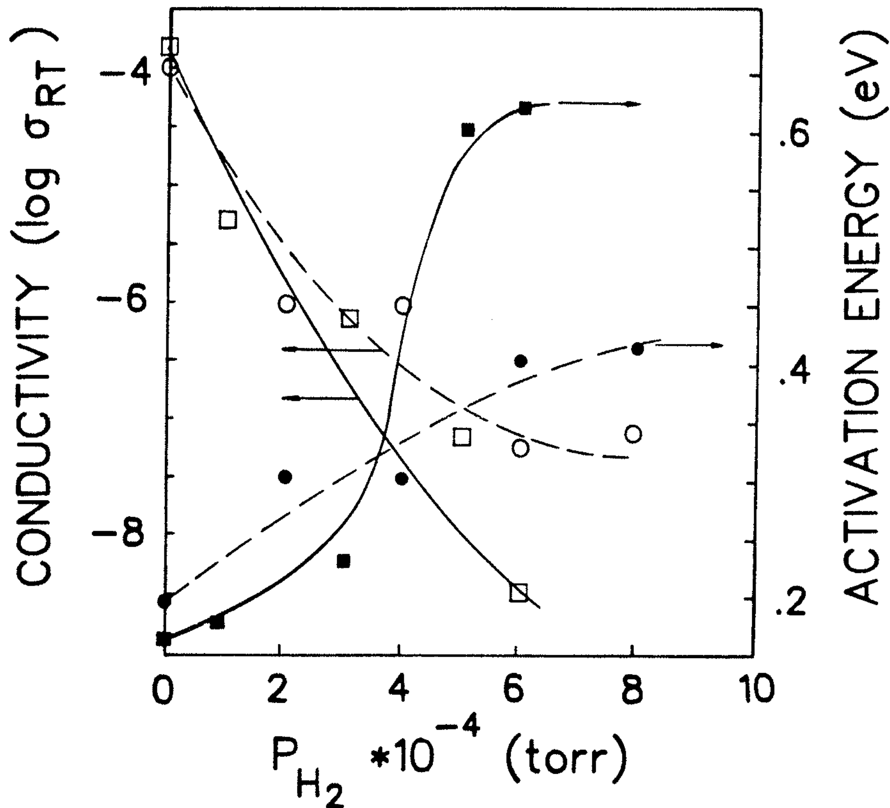

Figure 2.3: Conductivity and activation energy vs. H_2 partial pressure

It is not apparent to us what the exact process involved which causes the oxygen incorporation to increase with hydrogen partial pressure. However, Ishikawa [34] has found using Rutherford backscattering analysis that in his samples, oxygen concentration increased from 0.5 at. % at the substrate surface to 15 at. % near the surface. This variation in oxygen concentration was attributed to the outgassing of the chamber during the deposition as a result

of the heat generated by the electron-beam. In our results, the degree of oxygen incorporation increased with H_2 partial pressure, although a depth profile of the oxygen content was not available. This can be attributed to a combination of the deposition rate and system outgassing. When the partial pressure is increased, the number of collisions increases, resulting in a reduced deposition rate. Therefore, the deposition time was longer, permitting increased amounts of outgassing to occur. Due to the 200°C bakeout limit, the system could never be completely outgassed. This was corroborated by increased contaminant partial pressure measured by a Varian partial-pressure gauge. Methods to alleviate this problem were taken in the form of a pre-deposition evaporation. Preliminary evidence indicates an improvement, although the problem was never completely eliminated.

Figure 2.4 illustrates the dependence of the refractive index (n) at relatively long wavelengths (2.5 μm) upon the partial pressure, again for samples prepared with probe voltages of 0 and 200 V. The initial decrease in n is attributed to the saturation of dangling bonds with a corresponding decrease in the ESR signal [40]. Due to the exceptionally high defect density of e-beam evaporated a-Si [41], almost any element or compound incorporated into the growing film will reduce the long wavelength refractive index. For films prepared with zero probe voltage, there is a significant decrease in n below 3.0 for films evaporated in a

partial pressure of H_2 greater than 4 x 10^{-4} torr. This evidence supports arguments that substantial oxygen [27] is being incorporated into the growing film and plays a major role in determining the characteristics of the films. On the other hand, for films prepared at a 200 V probe potential, the refractive index tends to a value of 3.0, comparable to r.f. glow-discharge produced films. These results offer evidence that the probe is effective in incorporating atomic hydrogen into the growing film. Thus it can be argued that, as expected, atomic hydrogen is much more effective than molecular hydrogen in suppressing the effects of impurities such as oxygen.

From spectrally-resolved ellipsometry and spectrophotometry results, we have inferred the value of the optical energy gap E_{opt}, by assuming parabolic bands for the extended states in the form of [27]

$$\alpha = \frac{B^2(h\nu - E_{opt})^2}{h\nu} \qquad (2.1)$$

The dependence of E_{opt} upon the hydrogen partial pressure and probe voltage is shown in Fig. 2.5. The films prepared in the reactive atmosphere (probe voltage of 200 V) consistently demonstrated a larger optical gap than their counterparts prepared with zero probe voltage. The difference in E_{opt} in the two cases, at a given partial pressure of H_2,

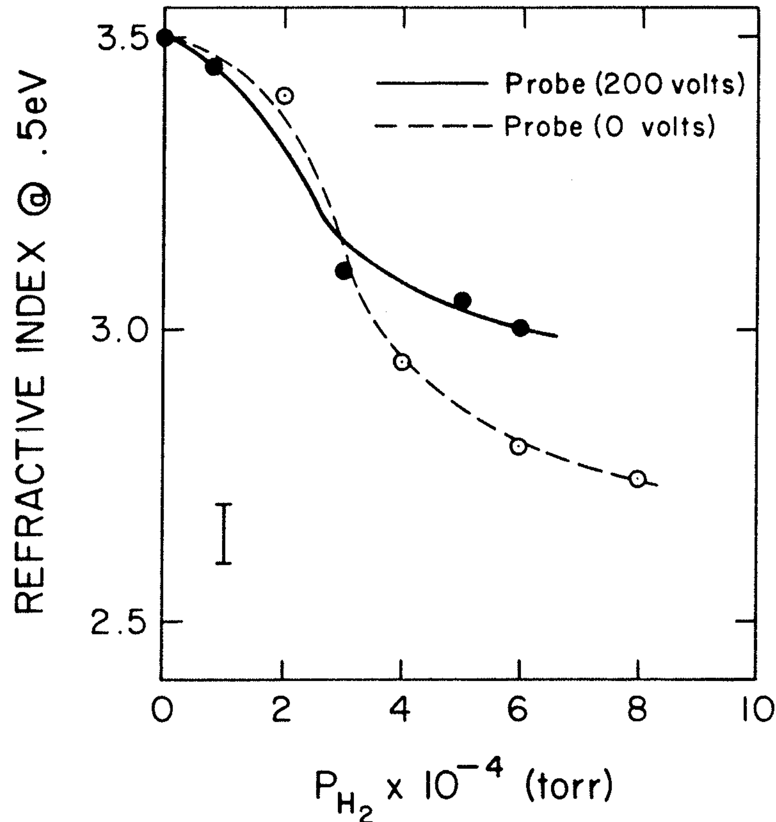

Figure 2.4: Refractive index vs. H_2 partial pressure

provides additional evidence that atomic hydrogen is being incorporated into the films. This can be compared with the usual value of E_{opt} for a-Si:H between 1.6 and 1.8eV whereas $E_{opt} \cong$ 1.25eV for a-Si films. Qualitatively, the Si-H bonds are expected to be somewhat stronger than a network of Si-H -Si or Si-Si bonds and are responsible for the observed difference in E_{opt}. One always observes an increase in E_{opt} when alloying adds stronger bonds to the amorphous silicon network. This is true for silicon-hydrogen alloys since the Si-H bond energy is 77.2 kCal/mole whereas that of a Si-Si

bond is 54 kCal/mole. On the other hand, structural defects tend to decrease E_{opt}. This line of reasoning is consistent with the quantum-well model presented by Brodsky [42].

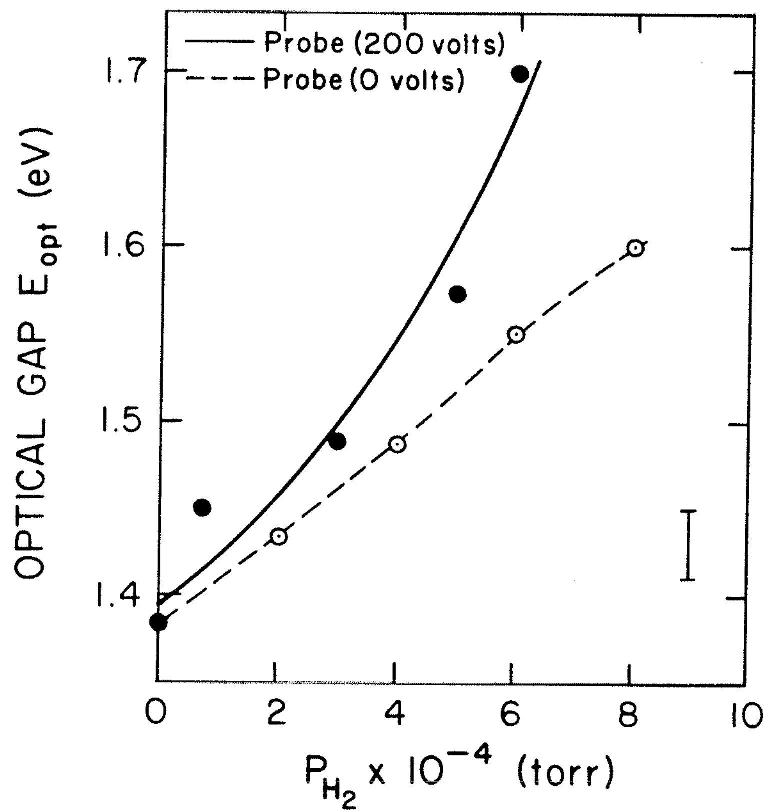

Figure 2.5: Optical gap vs. H_2 partial pressure

2.1.4 Further Results

Several other preliminary results determined with the collaboration of other investigators (M.S. Mathur, T.V. Herak) are now briefly reported. The morphology of the deposited films has been confirmed. This has been determined from measurements by Raman spectroscopy. The spectrum displayed a peak at 480 cm^{-1}, indicative of amorphous silicon, whereas the crystalline peak at 530 cm^{-1} was nonexistent.

Recently it has been found that at the low probe voltages, hydrogen is incorporated primarily in the molecular form. However, the results indicate that primarily atomic hydrogen is incorporated at high probe voltages. This has been determined by thermal annealing studies. Kniffler et. al. [43] have shown that by thermal annealing of an a-Si:H sample, the dark conductivity as a function of temperature decreases from 10^{-5} to 10^{-9} S cm^{-1} before it increases at temperatures over 300°C. The interpretation follows the reasoning that the molecular hydrogen forms atomic hydrogen and assists in the passivation of dangling bonds before the temperature is raised to a level at which the hydrogen begins to diffuse from the sample. Herak (unpublished results) has shown the same phenomena with samples prepared by ARE at low probe voltages. However, this phenomenon was very weak or non-existent when high

probe voltages were used. These results have also been confirmed for the case of laser annealing. A qualitative increase in E_{opt} was observed for samples prepared under low voltage conditions whereas the converse was observed for r.f. glow-discharge samples.

Chapter III

HYDROGENATED AMORPHOUS SILICON FOR ARCHIVAL STORAGE

3.1 ARCHIVAL STORAGE TECHNIQUES

The development of modern computer systems must contend with the seemingly insatiable demand for increased storage facilities. It now appears, however, that significant improvements in magnetic storage media are becoming increasingly difficult. On the other hand, optical storage systems provide a significant increase in ultimate storage capacities.

The ultimate density of information storage using optical techniques is nearly two orders of magnitude greater than that of magnetic media. The limitations in storage density are derived from physical and performance phenomena. Optical systems offer safe data storage for greater than 10 years as opposed to the 2-3 year shelf life of magnetic media. Another advantage of optical storage is the larger film-head distance, which increases the lifetime of the film. Due to the cost-effectiveness of optical storage media (price per bit more than 3 orders of magnitude below magnetic media) and to access times rivaling those of

magnetic media, archival storage devices offer a viable solution to the increased storage demands. Although optical storage technology has been in the laboratory stage for many years, it is finally entering the consumer market [45,44]. The most recent storage device is now capable of 500 Mbits per square inch [45].

Present state-of-the-art optical storage technology provides for write-once capabilities only. It has been the general consensus of the storage community that optical storage for archival purposes would be sufficient. The primary justification for this attitude was due to the low price of optical storage media, the difficulty it would encounter in competition with magnetic media and a general skepticism in the ability to produce methods of reversible optical storage. However, recent developments in magneto-optical and phase change materials establish the possibilities for erasable optical storage devices.

Various material systems have been explored for write-once optical storage applications. Four criteria are important for write-once materials. First, the material must match the wavelength of the laser chosen. The material must be stable for long periods of time (> 10 years) and provide a high signal to noise ratio (SNR). The material should also be mass producible.

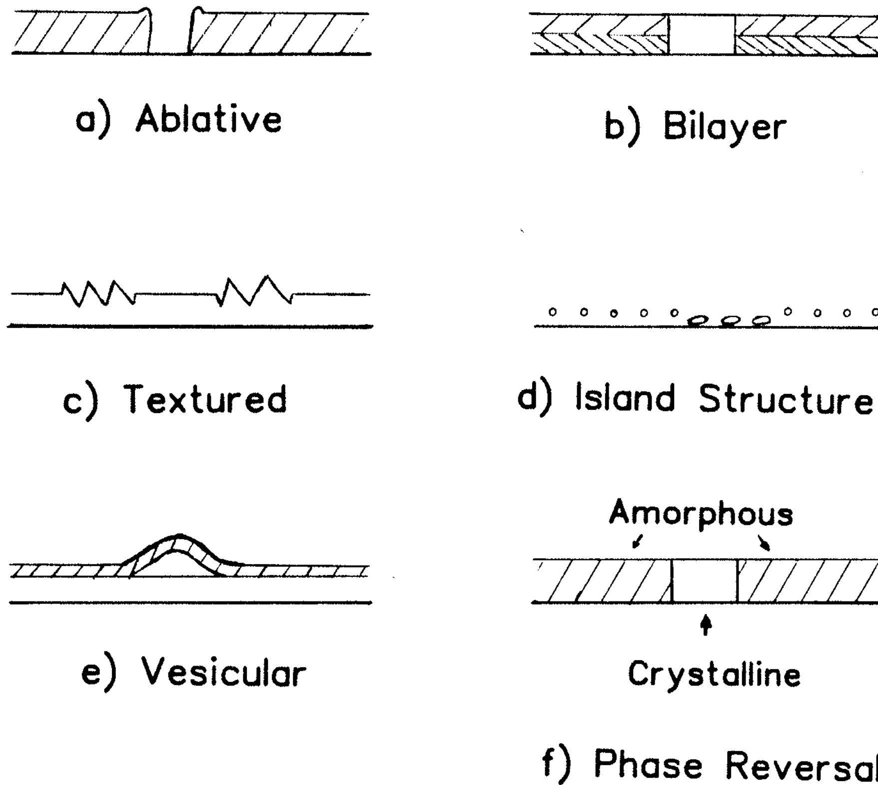

Figure 3.1: Writing Mechanisms for Storage Systems

Writing mechanisms chosen must be correlated with the film material in order to best satisfy the above criterion. In Fig. 3.1, 6 different writing mechanisms are illustrated [45]. Of these, the ablative technique has been the most popular due to its high SNR capabilities. The ablative procedure is accomplished by physical film removal. This is performed by either a melting/pullback or evaporation of the film at the point of processing. The primary film materials used for ablative processing have been Te and Te alloys including the elements Se, As, Sb or C [45]. The other writing mechanisms have not been investigated as thoroughly as the ablative procedure. Materials used for these systems

have included RhSi for bilayer processing, Ge for textured, Au islands for the island process. Au alloys on polymer films have been used for the bubbling (vesicular) technique and TeO has been studied for the phase-reversal method [45]. At present, several of the above writing mechanisms are entering the market. Recently, the use of a-Si:H has been proposed by several groups. Ablative [47,48,49], bubbling [48] and phase reversal [48] techniques have been investigated. The application of a-Si:H for archival storage media is still, at present, in the laboratory stage.

Present state-of-the-art optical storage systems are capable of generating bit cell sizes on the order of 1 μm square. The primary limitations appear to be the diffraction limitations associated with optical phenomena and the thermal profiles of the heated materials [50].

For the purposes of increasing the information storage density and the decrease of write power requirements, new writing mechanisms have been developed in our laboratory [2,3]. The writing tools consist of either a laser or an electron-beam. The use of electron beams to record and retrieve information promises to result in extremely dense data storage devices. The most straightforward write mechanism using electron beams is that of micro-machining a target surface in an ablative manner. In contrast, our proposed writing mechanism is shown to involve the simple

release of hydrogen from the a-Si:H network upon irradiation of the film. These writing techniques use considerably less power than previous a-Si:H based system requirements [2]. The predicted physical bit size is 1 μm and 0.01 μm for laser and electron-beam processing respectively.

3.2 NEW STORAGE METHODS USING A-SI:H

Recently a-Si has emerged as a candidate for an archival storage medium. Mechanisms for optical storage in a-Si that depend on optically-induced amorphous to polycrystalline transitions [48] and release of hydrogen from a-Si:H to produce either bubbling or ablative hole formation [51,47,49] have been proposed.

Additional mechanisms by which a-Si:H thin films can function as high-density archival storage media can be derived from optical and electron-beam addressed systems. The experiments described are concerned with the modifications to the bulk reflectivity and to the conductivity of a-Si:H as a result of the release of hydrogen from the films induced by either laser or electron-beam irradiation. With sufficiently low write power densities, these mechanisms do not appear to result in the rupture or distortion of the material. This indicates the potential reversability of the irradiation by rehydrogenation, although rehydrogenation was not performed in the present study. The bulk changes in the

electrical and optical properties provide the mechanism for interrogation of the stored information.

3.2.1 Experimental Techniques

The a-Si:H films were deposited in a conventional radio-frequency glow-discharge system at a power density of 0.1W cm^{-1} and a pressure of 0.1 torr in a SiH_4/H_2 atmosphere (1/1 ratio) on quartz substrates at a substrate temperature of 200°C. Typical film thicknesses were approximately 0.3 μm.

The optically-induced exo-diffusion of hydrogen was accomplished using an Argon laser (514 nm) in a CW-scanning mode over a relatively large area (100 μm x 2 cm. regions) for times of typically 5 minutes. The laser power was varied over the range of 100 mW to 1 W. This implies a power density more than an order of magnitude lower than that used for ablative write mechanisms [2]. Another departure from the conditions of the ablative a-Si removal work was that r.f. glow-discharge a-Si:H films on quartz substrates rather than reactively-sputtered films on glass substrates were employed. The major difference here is that the thermal coefficient of expansion of Si is much closer to quartz than to glass. These conditions may have contributed to the uniform changes in electrical and optical properties and coupled with the lower optical power densities, may

prohibit structural deformations that accompanied the results of other investigators.

The hydrogen evolution was also observed directly by in-situ measurements using mass-spectrometry during electron-beam irradiation of the a-Si:H material while under high vacuum conditions. These measurements, however, were made in a qualitative manner and the quantitative results have not been compiled, although Fritzsche et. al. [52] have demonstrated the accuracy of such a technique. Thermal annealing was also performed in order to study the bulk effects of hydrogen evolution, in particular the changes in conductivity.

3.2.2 Experimental Results

In Fig. 3.2, the change in reflectivity (ΔR) as a function of the total Ar laser power is shown. The cases of pulsed or continuous irradiation are illustrated. This demonstrates the capability to produce large changes in reflectivity without film damage. When the Ar laser power was increased above the values indicated in Fig. 3.2, the film displayed evidence of damage and in some cases crystallization was observed.

In Fig. 3.3 the dependance of optical reflectivity and electrical conductivity upon the hydrogen content of the a-Si:H films remaining after either Ar laser irradiation or

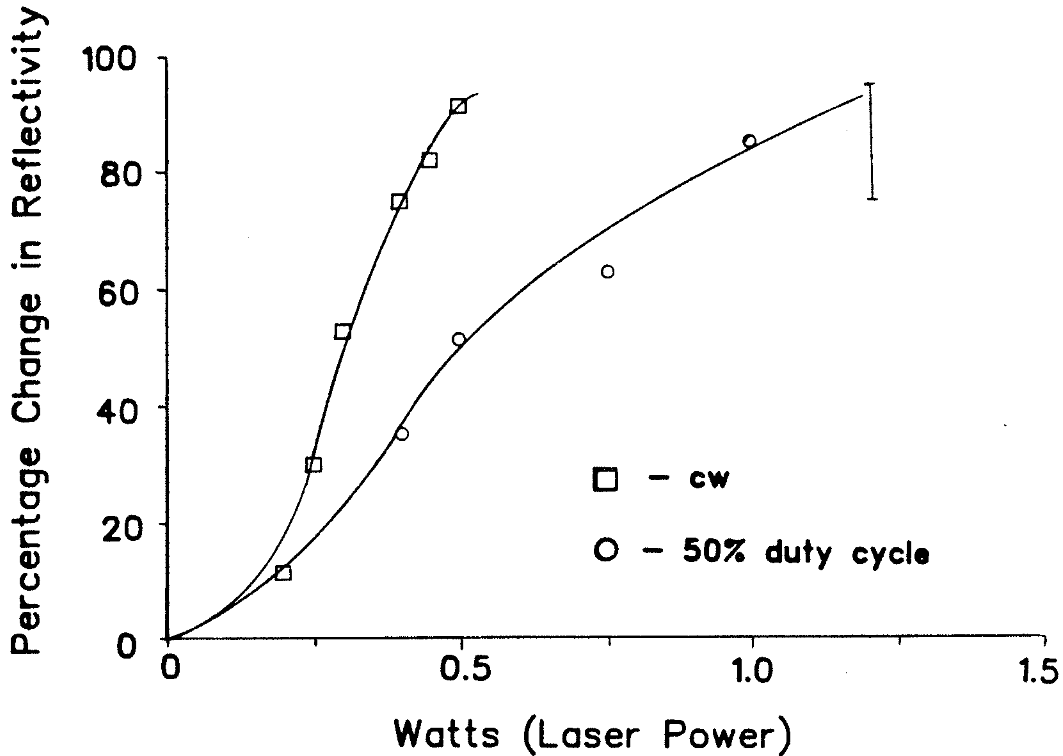

Figure 3.2: Reflectivity vs. Ar Laser Power

thermal annealing is shown. The reflectivity was measured at a wavelength of 632.8 nm, and is presented in Fig. 3.3 as $\Delta R/R$ where ΔR is the induced reflectivity change. The hydrogen content could be controlled either by the power of the Ar laser or the duration of irradiation. This hydrogen content was calibrated by comparison with identical films in which the H effusion from the films was stimulated thermally at 400°C. In the thermal evolution experiments, the H/Si

ratio in the films was established by comparison of the electrical and optical properties with those reported by other investigators [53,54]. This was subsequently confirmed by infrared absorption measurements of the H content [4].

It is interesting to note that for the given film thickness of 0.3 μm, and for the wavelength used in the reflectivity measurements, an amorphous to crystalline phase change would cause the opposite trend to that of Fig. 3.3. That is, the reflectivity would increase rather than decrease as illustrated. Although no structural damage was observed by scanning electron microscopy, the resolution of the SEM was limited to approximately 1 μm.

It is important to realize that the degree of change in the reflectivity as well as the direction of change induced by the hydrogen evolution is a damped periodic function of the optical path length through the film (determined by λ and the film thickness). Independent measurements of the refractive index and extinction coefficient for the a-Si:H materials were recorded and are presented in Fig. 3.4. These results are in reasonable agreement with earlier studies of sputtered a-Si:H [55], and have been used to predict the reflectivity changes as a function of film thickness, wavelength, and H content. It has also been found that the H content is the predominant factor in deter-

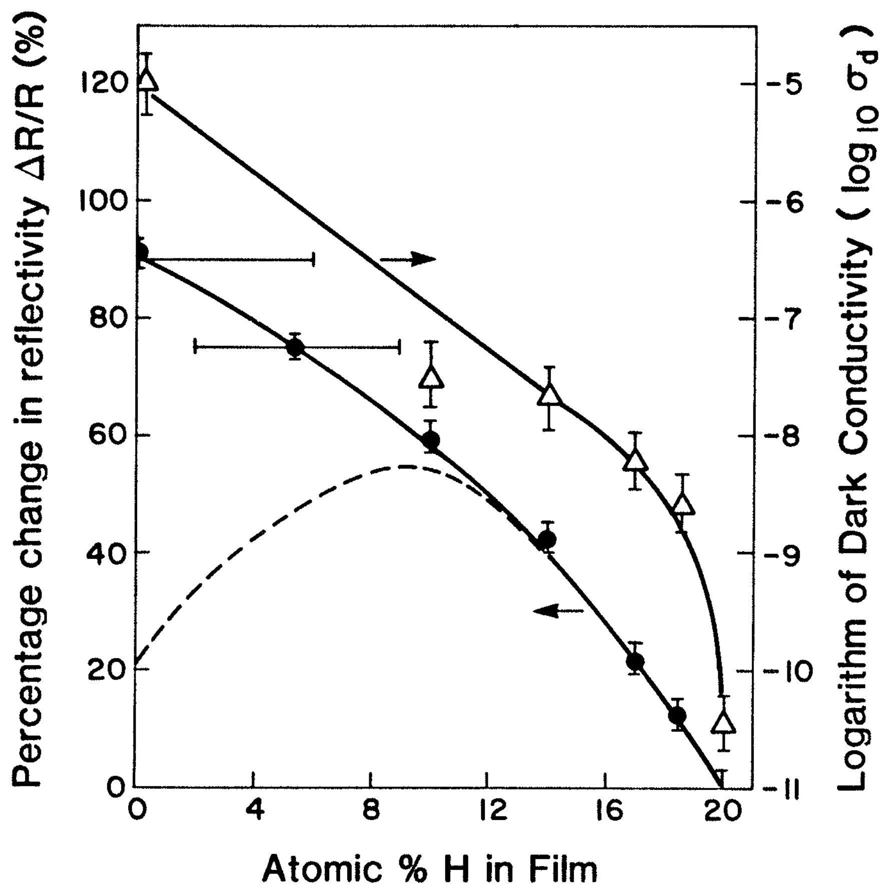

Figure 3.3: Reflectivity and conductivity vs atomic H content. Reflectivity ($\Delta R/R$) measured at $\lambda = 632.8$ nm with a 0.3 μm thick a-Si:H film. Dashed line indicates theoretical calculation based upon single two layer model (Appendix A).

mining n and k. Alternative fabrication techniques and process parameters have a minimal effect on n and k except to the extent they effect the H content. Further discussion on this is found in Chapter 4. An optical model of the

film-substrate system [56], described in detail in Appendix A, has been employed which includes the absorption in the a-Si:H film. These calculations are in excellent agreement with experiments in which the H evolution was induced thermally, over a range of film thicknesses, which suggest that the hydrogen content remaining in the film is uniformly distributed in that case.

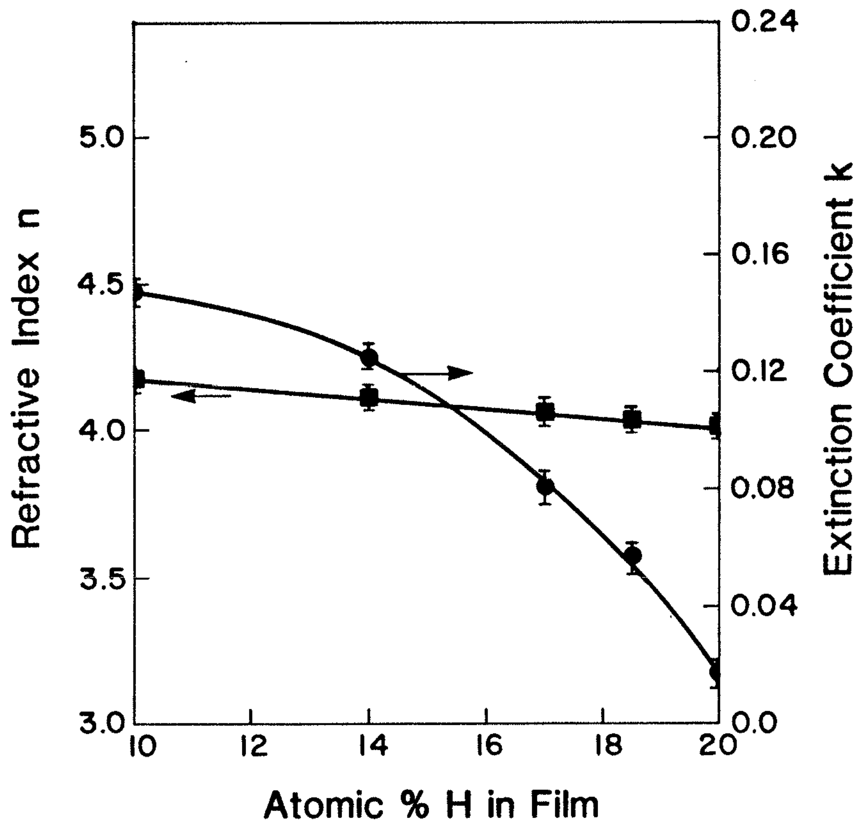

Figure 3.4: Refractive index and extinction coeff. vs. atomic H content. (a-Si:H film thickness d = 0.3 μm)

For the laser-induced changes in reflectivity in Fig. 3.3 there is agreement with the optical model (same n and k values for a given H content) for the larger H concentrations (>10 at. % H). The dashed line in Fig. 3.3 shows the model predictions. Sustained laser irradiation which further reduces the H content results in non-uniform optical properties throughout the film. This is a fortunate development since it increases the desired effect on ΔR as is evident in Fig. 3.3.

The hydrogen effusion discussed above was also induced by electron-beam irradiation at an energy of 4 keV, with a change in the monitored hydrogen partial pressure from 2.5×10^{-8} torr to 4.5×10^{-7} torr during H evolution. The conductivity changes in Fig. 3.3 suggest a means by which the stored information can be interrogated by an electron-beam. This would be similar to the method by which photoconductive regions are identified in a vidicon tube.

3.2.3 Theoretical Evaluation

3.2.3.1 Laser Processing

The primary factor changing the reflectivity upon annealing is the extinction coefficient k (which determines the optical absorption coefficient α). As can be observed in Fig. 3.4, k is strongly dependent on the hydrogen

content. The effect on k is a result of the increase in the bandgap density of states resulting in a reduced optical gap. Usually, for good quality films, E_{opt} = 1.8 for ≅20 % at. H and E_{opt} = 1.3-1.4 for 0 % at. H. Theoretical values for reflection can be derived from the frontside reflectivity calculations presented in Appendix A. In Fig. 3.5, the reflectivity is presented as a function of the thickness for the cases of 20, 10, and 0 % at. H content. The solid arrow in Fig. 3.5 illustrates the large change in reflectivity. The maximum change in reflectivity is dependent on the film thickness and the initial and final hydrogen concentrations. The transition from position 1 to position 2 in Fig. 3.5 demonstrates a 50% change in hydrogen content. However, if all the hydrogen is evolved, the reflectivity change is limited to a transition to position 3. Then the question arises as to why or how the large changes in reflectivity observed experimentally were achieved. Beyer and Wagner [54] have demonstrated that the evolution of hydrogen can result in a reduction in film thickness of up to 10 %. As a result, the optical thickness is also reduced causing the larger reflectivity change illustrated by the transition to position 4 in Fig. 3.5. As the exact value of hydrogen content was not known for the specific results demonstrating the large reflectivity changes, the rather large error bars were inserted in Fig. 3.3.

It should be noted that these large changes in reflectivity are not a result of a solid phase change. Further, although it appears a possible physical thickness change is occurring, this in no way prohibits re-hydrogenation.

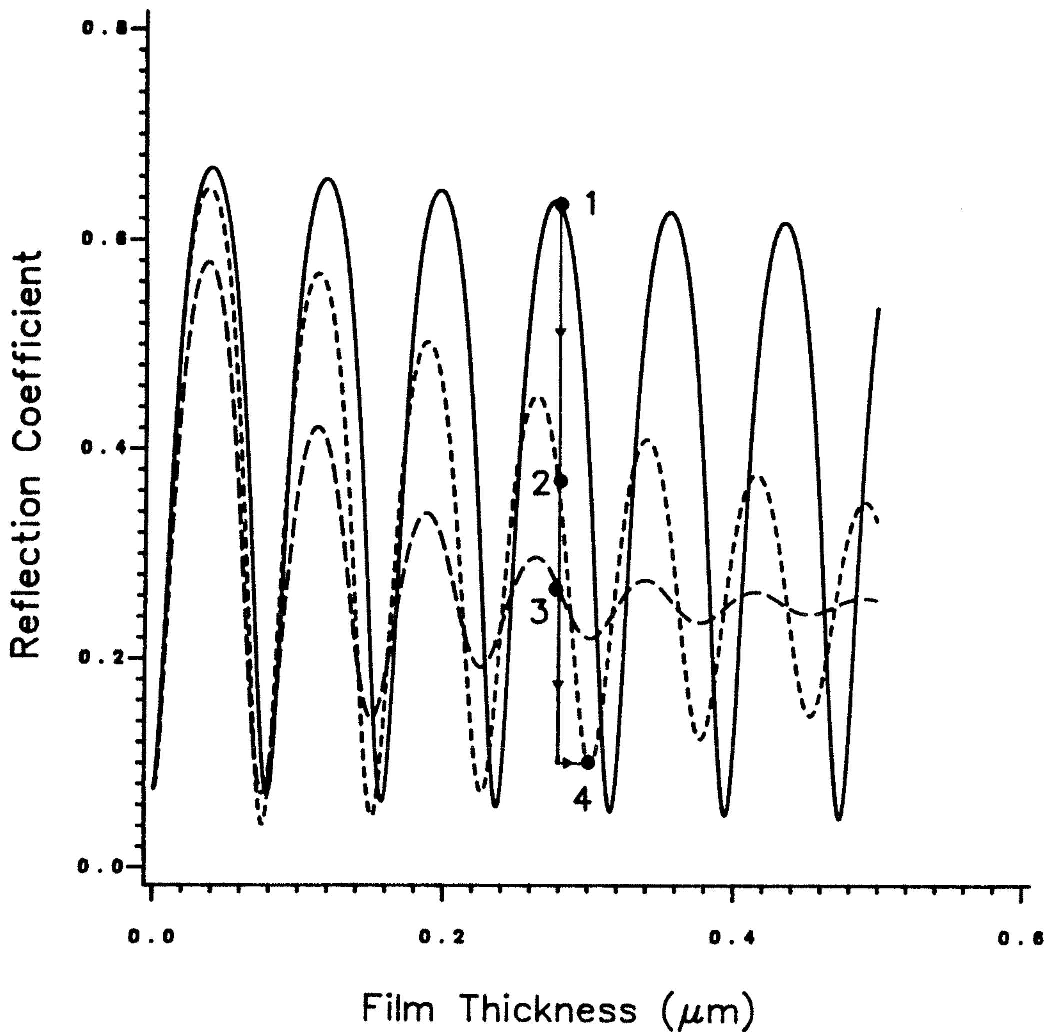

Figure 3.5: Reflectivity vs. thickness. The three patterns shown are representative of 20, 10, and 0 at. % H for the solid, short dashed and long dashed curves respectively.

3.2.3.2 Electron-beam Processing

The primary factor affecting the conductivity upon the release of hydrogen is the increase in the energy gap density of states. This is a result of the hydrogen evolution which increases the number of dangling bonds and decreases the activation energy, with a corresponding decrease in E_{act} resulting in an increased conductivity. As seen in Fig. 3.5, high SNRs are possible using e-beam processing since more than 4 orders of magnitude changes in conductivity can be obtained.

The electron beams which may be prepared at present are capable of focusing to less than 1 nm diameter. As a result, high storage densities are anticipated. However, to generate beams with such focii, the beam window is limited to approximately 1 cm square. As a result, a mechanical means of window movement would be necessary.

3.2.4 Storage Density Limitations

As an optical storage medium, a-Si:H which undergoes a process of laser or electron-beam-induced hydrogen evolution is expected to have an ultimate storage density limited by the following considerations. As the medium is locally elevated in temperature by the deposited energy from the beam, the material surrounding the cylinder will also experience a temperature rise due to thermal conduction.

This process has been modelled by Lax [57] for the laser irradiation and by Schiller [58] and El-Kareh et. al. [50] for the electron-beam irradiation.

3.2.4.1 Laser Processing

We assume a Gaussian intensity distribution,

$$I = I_0 e^{(-r^2/w^2)} \tag{3.1}$$

where r is the radial distance from the center and w is the beam width. The energy absorbed per unit volume per second is defined by

$$G = \alpha e^{-\alpha z} I_0 f(r/w) \tag{3.2}$$

where α is the absorption coefficient and z is the depth parameter. The total incident power can be calculated as

$$P = I_0 \int_0^\infty f(R) 2\pi r dr \equiv I_0 \pi w^2 \tag{3.3}$$

for the Gaussian case. Using the normalization factor

N(R,Z,W) where

$$R = r/w, \quad Z = z/w, \quad W = \alpha w \tag{3.4}$$

the temperature rise is written as

$$T = T_{max} N(R,Z,W), \quad T_{max} = \frac{P}{2\pi K} < 1/r > \tag{3.5}$$

The value of <1/r> is the mean inverse distance from the beam center at the surface. The normalization factor is calculated such that the boundary condition

$$\lim_{W \to \infty} N(0,0,W) = 1 \tag{3.6}$$

is met. The solution to the standard heat equation

$$C \frac{\partial T}{\partial t} = -div(-K \nabla T) + G \tag{3.7}$$

where

C = heat capacity
K = thermal conductivity
T = temperature

and G is given by Eqn. 3.2, has been calculated by Lax [57] resulting in the time-independent solution of the normalization factor as

$$N(R,Z,W) = \frac{w}{\int_0^{\infty} F(\lambda)\, d\lambda} \int_0^{\infty} J_0(\lambda R) F(\lambda) \frac{we^{-\lambda z} - \lambda e^{-wz}}{w^2 - \lambda^2}\, d\lambda \tag{3.8}$$

where

$$F(\lambda) = \int_0^{\infty} f(R) J_0(\lambda R)\, dR \tag{3.9}$$

and

$$F(\lambda) = \frac{e^{-\lambda^2/4}}{2} \tag{3.10}$$

for the Gaussian case.

Using the above solution, the temperature profile for laser irradiation has been calculated. The maximum temperature rise is generated at the surface and as a result, using the values of

$$Z = 0$$
$$\alpha = 10^5\ cm^{-1} \quad (for\ \lambda = 514\ nm)$$
$$T(R=0, Z=0, W=0) = 1$$

the normalized temperature has been determined assuming the worst case conditions of steady state irradiation. The resultant temperature profile for laser annealing are as in Fig. 3.6. Assuming that the rate of H evolution is negligible below 400°C [54], and in view of the short irradiation times, these results indicate that the maximum storage densities are in the range of 10^9 bits per square inch for laser irradiation (cell size 1 μm, spot size 0.6 μm).

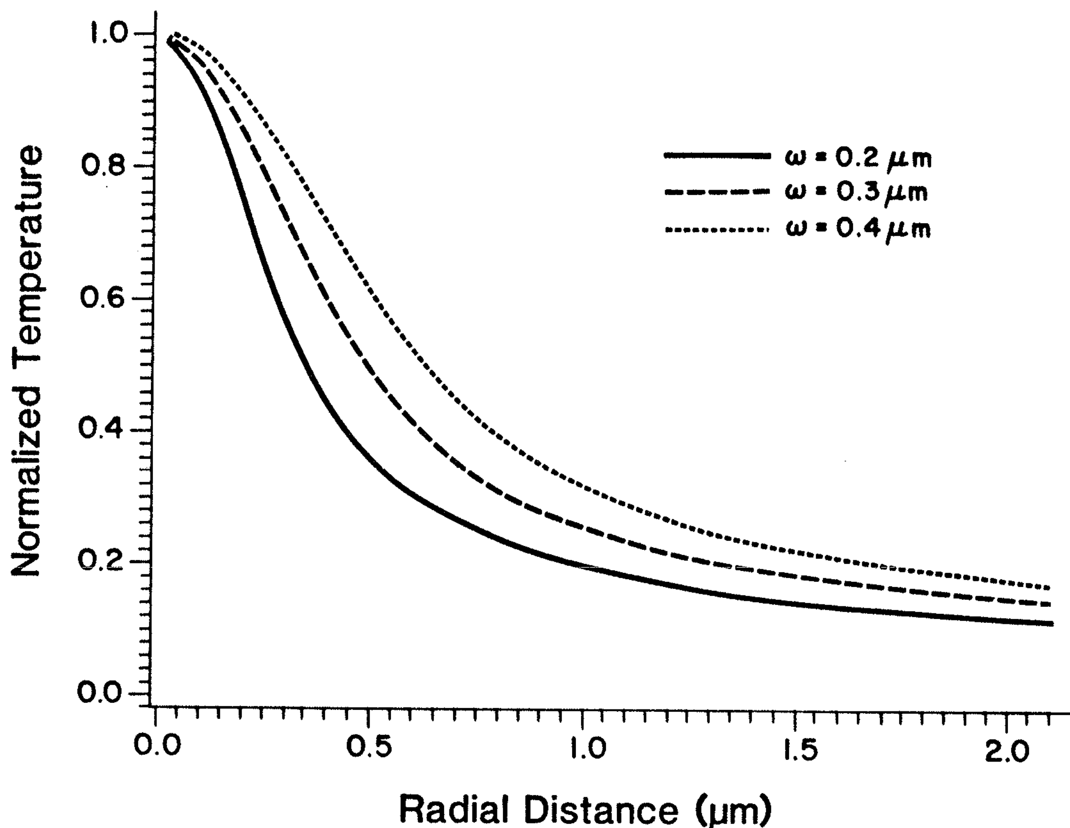

Figure 3.6: Temperature profile for laser annealing

3.2.4.2 Electron-beam Processing

Similar temperature distribution profiles were calculated for the electron-beam case. Due to the mass difference between electrons and atoms or molecules, many collisions are required for the electron to lose all of its energy. The electron range S is the distance into the film, perpendicular to the surface, within which the electrons lose virtually all their energy. S can be approximated as

$$S \approx 2.1x\,10^{-12}\frac{U_B^2}{\rho} \qquad 10\,keV \le eU_B \le 100\,keV \tag{3.11}$$

where U_B is the acceleration voltage and $\rho(g\ cm^{-3})$ is the material density [58]. Since the films to be used for the proposed archival storage systems are of the order of 0.1 μm thick, the acceleration voltage will necessarily be on the order of 2.5 keV. For increased power density, the acceleration voltage must be decreased or the current density must be increased. Using the characteristic times of

$$\tau_{t,S} = \frac{S^2}{4a} \tag{3.12}$$

$$\tau_{t,d_F} = \frac{d_F^2}{16a} \qquad (3.13)$$

described by Schiller, where

$a = \lambda/\rho c$
λ = thermal conductivity
ρ = material density
c = specific heat of the material
d_F = electron-beam focal spot diameter

the temperature profile becomes time independent when t (time) is greater than the lower of the two quantities, S and $d_F/2$. When the time exceeds the characteristic times described in Equations 3.12 and 3.13, the heat conduction causes an extension of the temperature field beyond the energy absorption limits defined by S and d_F. However, the maximum temperature remains an increasing function of time. Hence, when $r > d_F$, S the temperature distribution is given by

$$T(r) = \frac{P_0}{2\pi\lambda r}, \qquad t >> \tau_t \qquad (3.14)$$

where P_o is the beam power. As a result of the reduced electron-beam diameter, the maximum storage density is expected to be in the range of 10^{11} bits per square inch (cell size 0.1 µm, spot size 0.01 µm). The above limita-

tions are no worse than those which arise from diffraction effects. It is further expected that some fraction of the evolved hydrogen will be incorporated around the edges of the programmed area, leading to a self-enhancing contrast mechanism.

3.2.5 Discussion

It has already been stated that the thermal or laser annealing process was performed below the crystallization temperature. In the work of Shanks and Ley [47], results showed that pinhole formation due to a combination of hydrogen release, bubbling, and bubble bursting occurred at temperatures above 350°C. McMillan [59] experienced a large and rather sudden increase in H diffusion at 375°C (thermal anneal) whereas the principle H diffusion occurred at 600°C. This can, in part, contribute to the mechanism for sudden pinhole formation above 350°C. This was also observed in the present study during thermal annealing of glass substrate samples. However, this effect was not as evident for the quartz substrate samples. This is attributed to the differences in the thermal expansion coefficients. The results of laser annealing did not demonstrate any pinhole formation. Although relatively high temperatures ($\cong$ 500°C) are required to activate the diffusion of hydrogen, it is believed that the effects of local excitation differ from those in bulk effects. In the bulk process, the hydrogen

must diffuse outwards or create bubbles and possible pinhole bursts. However, under localized heating, the hydrogen is also permitted to diffuse to the neighboring regions, preventing any sudden physical damage. Therefore, it is believed that under local excitation by a laser or by an electron-beam, large changes in reflectivity and conductivity can be experienced without a significant impact on the film structure.

The possibility also exists for inducing an altered amorphous state as a writing mechanism. This is based on the existence of the many possible amorphous states having different minimum energy configurations. The lowest energy configuration coincides with the crystalline state. However, instead of a complete amorphous to crystalline phase change, it may be possible to determine an alternate writing mechanism based on an inter-amorphous state transition. The primary advantage of such a method would be the low power requirements and the relatively minor changes in film morphology. It may also be possible to derive more than two useable stable amorphous states for this purpose, enabling the development of a multi-leveled storage device, although this idea is purely hypothetical at present.

Chapter IV

TECHNIQUES FOR MONITORING FILM FABRICATION

Thin film measurement systems are concerned with the empirical determination of the physical parameters related to mechanical, electrical, magnetic and optical properties. These parameters are measured either in-situ or post-fabrication. The primary parameter for thin films is their thickness.

In the case of hydrogenated amorphous silicon, the important physical quantities for preliminary investigation include:

Mechanical Properties : Thickness
Electrical Properties : E_{act}, σ_d , σ_{ph}
Optical Properties : n, k, E_{opt}

The electronic and optical properties of hydrogenated amorphous silicon films are known to be strongly correlated with the hydrogen concentration incorporated into the film during the fabrication process. This degree of hydrogen incorporation is in turn dependent on the fabrication technique (glow-discharge in silane, vacuum evaporation in a hydrogen atmosphere, radio-frequency sputtering of silicon

in hydrogen, etc.) and upon the deposition parameters (substrate temperature, chamber pressure, gas flow, ambient gas mixture, etc.). A method to monitor the degree of hydrogen incorporation during the fabrication process is clearly a desirable ingredient in the procedure by which film properties are optimized for a given device application.

4.1 IN-SITU MONITORING OF HYDROGEN INCORPORATION IN A-SI:H

An optical mechanism based upon temporal changes in reflectivity and transmission during the growth of a-Si:H thin films is shown in this chapter to provide for an accurate determination of the degree of hydrogen incorporation, as well as the growth rate of the growing film. This mechanism, described experimentally and modelled phenomenologically, is expected to provide a basis for the in-situ monitoring of hydrogen incorporation with process parameters.

Methods of film thickness monitoring in-situ have been developed previously and are described by Chopra [29]. Techniques using film resistance, capacitance, vapor ionization, micro-balances, quartz-crystal resonance, or optical interference have been employed. However, most of these methods are not yet capable of determining other important parameters, specifically the hydrogen content.

A method which provides for in-situ measurements of hydrogen incorporation and growth rate of a-Si:H has been

developed in this work based upon non-destructive measurements of optical reflectivity [4]. These measurements are based on the predictable dependence of the optical constants (refractive index n and extinction coefficient k) upon the hydrogen content of a-Si:H. Although these optical constants are also dependent on other physical parameters such as bonding configurations, and deposition conditions, an extensive literature search has indicated that the primary factor in determining n and k in the wavelength region of interest is the concentration of H in the films alone. The correlation of the H content with the absorption coefficient was verified for film fabrication techniques including radio-frequency glow-discharge deposition in SiH_4/H_2, microwave plasma deposition in SiH_4/H_2 gas mixtures [17], and activated reactive evaporation of a-Si in a H atmosphere [4].

4.1.1 Experimental Techniques

The a-Si:H thin films to be described below were prepared under the following conditions (a) radio-frequency glow-discharge in SiH_4; substrate temperature 200°C, rf power density 0.1 Wcm^{-1}, 1/1 SiH_4/H_2 ratio in deposition atmosphere; (b) electron-beam evaporation of silicon: H partial pressure = 0, substrate temperature 200°C; (c) microwave glow-discharge as described by Mejia et. al. [17] in 10% SiH /45% H /45% Ar, total flow rate 30 sccm, microwave power 45W, pressure 0.1 torr, substrate temperature 200°C.

The hydrogen content in the films was controlled in several ways. (i) materials fabricated with initially large H content (20%) (by method (a) above) were subjected to thermal annealing at 400°C for various time intervals as described by Beyer and Wagner [54]. (ii) hydrogen evolution was induced by processing with an Ar laser as described in Chapter 3, and (iii) the hydrogen initially incorporated into the films was varied by using different fabrication techniques or control of the deposition parameters for a given process.

The hydrogen content of the films was measured by the analysis of the 640 cm^{-1} band in the infrared-absorption spectra using the method described by Shanks et. al. [47]. The optical constants n and k were determined at $\lambda = 632.8$ nm by transmission and reflection measurements with a He-Ne laser source. The optical constants were found to be completely determined by the hydrogen content of the films alone, regardless of the fabrication method or parameters, within the limits of experimental error.

4.1.2 Experimental Results

On the basis of the dependence of n and k upon the hydrogen content, an optical model of thin a-Si:H films on quartz substrates has been employed, based upon the work of

Heavens [56]. The derivation of the model is presented in Appendix A. For convenience in process monitoring, both the optical model and the experiments described below correspond to the determination of reflectivity for backside illumination (the 632.8 nm radiation is incident upon the back of the quartz substrate). Reflectivity at all interfaces, multiple reflections within the film and optical absorption are considered explicitly. The predicted dependence of reflectivity upon thickness of the deposited a-Si:H film as calculated numerically is shown in Fig. 4.1.

The three curves in Fig. 4.1 correspond to 0, 10, and 20 % atomic hydrogen in a-Si:H which give rise to optical constants n and k of

$n = 4.2$	$k = 0.428$	(0 at. % H)
$n = 4.192$	$k = 0.148$	(10 at. % H)
$n = 4.01$	$k = 0.016$	(20 at. % H)

at a wavelength $\lambda = 632.8$ nm.

Fig. 4.2 shows the comparison between our experiments and the predictions of the model for a-Si:H films of various thicknesses prepared under two separate conditions : electron-beam evaporation without plasma assist, for which the H incorporation is negligible; and microwave plasma deposition in a 1/1 mixture of SiH_4/H_2 for which the atomic hydrogen content was determined by infrared absorption measurements to be 10% atomic hydrogen.

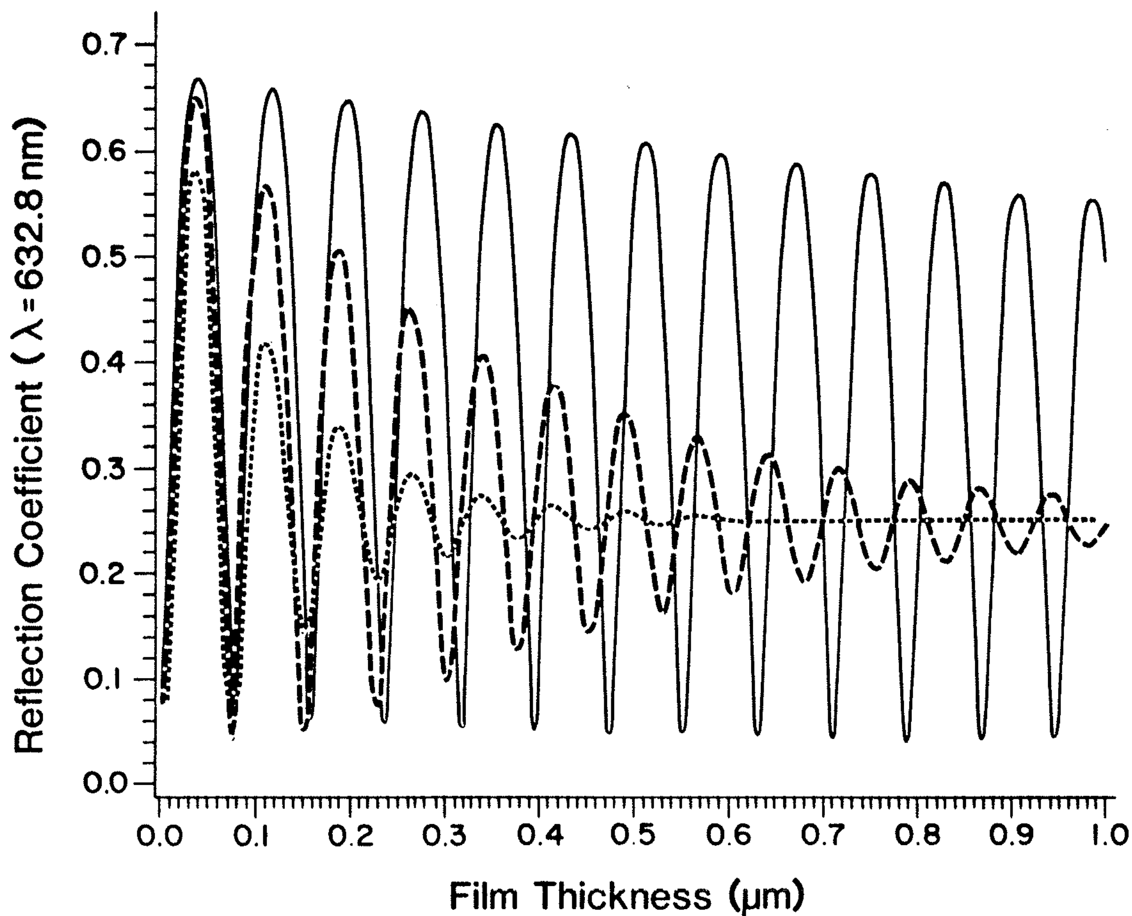

Figure 4.1: Reflection Coefficient vs. Film Thickness calculated at wavelength λ = 632.8 nm. The solid, long-dashed and short-dashed lines correspond to n=4.01, k=0.016; n=4.192, k=0.148; n=4.2, k=0.428 respectively, where n is the refractive index and k is the extinction coefficient. These curves are representative of optical parameters for 20, 10 and 0 at % H in a-Si:H films respectively.

Note that the validity of the present characterization technique rests upon the degree of correspondence between predictions and experiment in Figs. 4.2 (a) and (b) as the film thickness increases. The predictions are based on

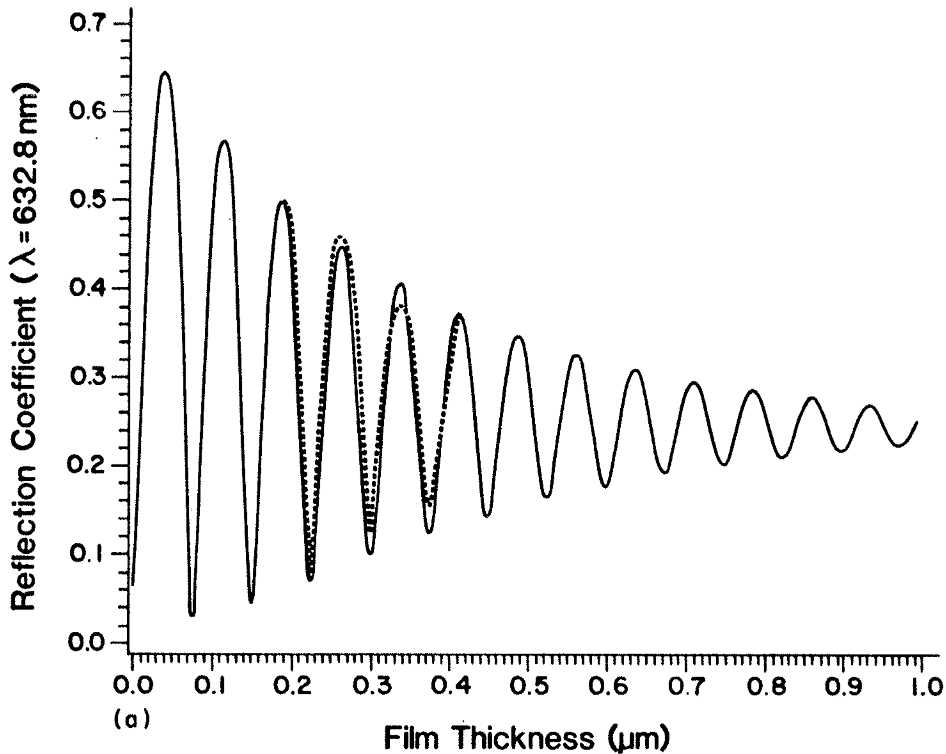

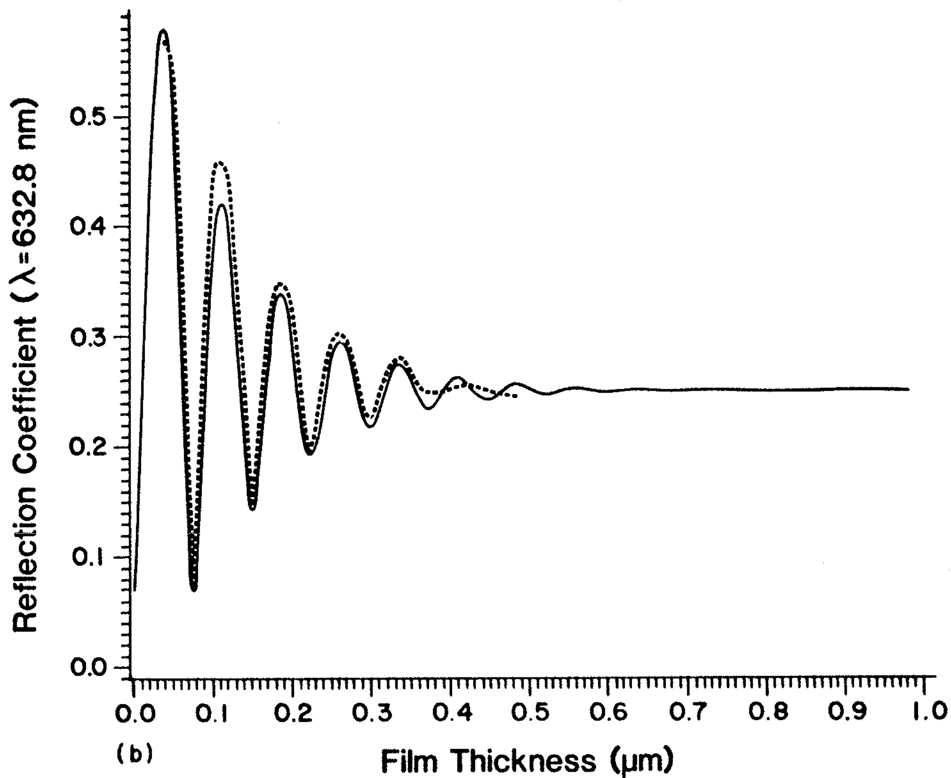

Figure 4.2: Experimental Reflection vs. Film Thickness. The solid line represents the predictions of the optical model and the dashed lines represent the experimental measurements, for (a) a-Si:H produced by microwave glow-discharge (10 at % H) and (b) a-Si produced by electron-beam evaporation in absence of hydrogen plasma (0 at % H).

measurements of n and k at a single film thickness, and the reasonable agreement in these figures with experimental measurements over a range of thicknesses substantiates the optical model. In particular, the assumption of uniform film properties in the optical model seems to be justified.

The strong dependence of the decay in the oscillations upon the H content in Fig. 4.1 is responsible for the utility of the present characterization technique. Secondary factors affecting results such as these are suppressed by the overwhelming dependence on the H concentration alone. The H content of a growing film can be determined with considerable accuracy by monitoring the rise and fall in the reflectivity as the film grows in thickness. The growth rate is also readily determined from n and λ alone; however, the relative insensitivity of n to H content (as compared to the dependence of k on H content) makes this determination essentially independent.

4.1.3 Determination of the Extinction Coefficient

The primary value of interest in this measurement technique is the extinction coefficient k. The optical constant k can be determined by two methods. The first method requires the measurement of the reflection and transmission coefficients and the film thickness. The second method

requires the measurement of the reflection coefficient and an approximate knowledge of the refractive index of the film.

Method One

Given the values of R, T, λ , and d (reflection, transmission, wavelength, thickness) the values of n and k can be determined by solving the optical equations in Appendix A in reverse. This, however, is practically impossible and there is no guarantee that the correct solution will be found. The procedure proposed, and demonstrated successfully, involves the estimation of a range of valid values for n and k. Although multiple solutions exist, a unique solution can be derived based on previous results. This is not unreasonable since the value of n does not vary significantly from 4.0 when $\lambda = 632.8$ nm. As for the value of k, the solution provides a nearly unique result.

The values of R and T are measured experimentally. However, since the extinction coefficient is not known, it is not obvious how these values can be normalized. We note that for high concentrations of hydrogen, the absorption of an a-Si:H film approaches that of a crystalline film. Therefore, we make the assumption that in the limit, for a high quality a-Si:H film, the absorption coefficient will approach that of the c-Si film. Using this assumption, we

now normalize our measured values of R and T to that of a c-Si sample of the same thickness. Therefore, knowing $n = 4.0$ and $k = 0.0151$ for c-Si, with $\lambda = 632.8$ nm and $d = 0.3$ μm, the calculations of Appendix A yield $R = 0.441$ and $T = 0.480$.

The iterative procedure in determining the values of n and k requires a 3-dimensional plot of the inverse error as a function of the estimated n and k. The inverse error is calculated as

$$IERR = \left[\sqrt{(R - R_0)^2 + (T - T_0)^2}\right]^{-1} \tag{4.1}$$

where R_o , T_o are normalized values and R , T are calculated from the estimated n and k. As an example, consider the inverse error plot of Fig. 4.3. The values of R_o and T_o were determined to be 0.332 and 0.413 respectively. The sample had a thickness of 0.3 μm.

We note that all inverse error peaks occur at a value of $k \cong 0.056$. The value of n is determined to be 4.04 as this is the best choice from those available based on published results by other investigators.

This method has been found to be quite successful. A similar approach has been demonstrated by Denton et. al. [60], with an attempt to eliminate the possibility of multiple solutions.

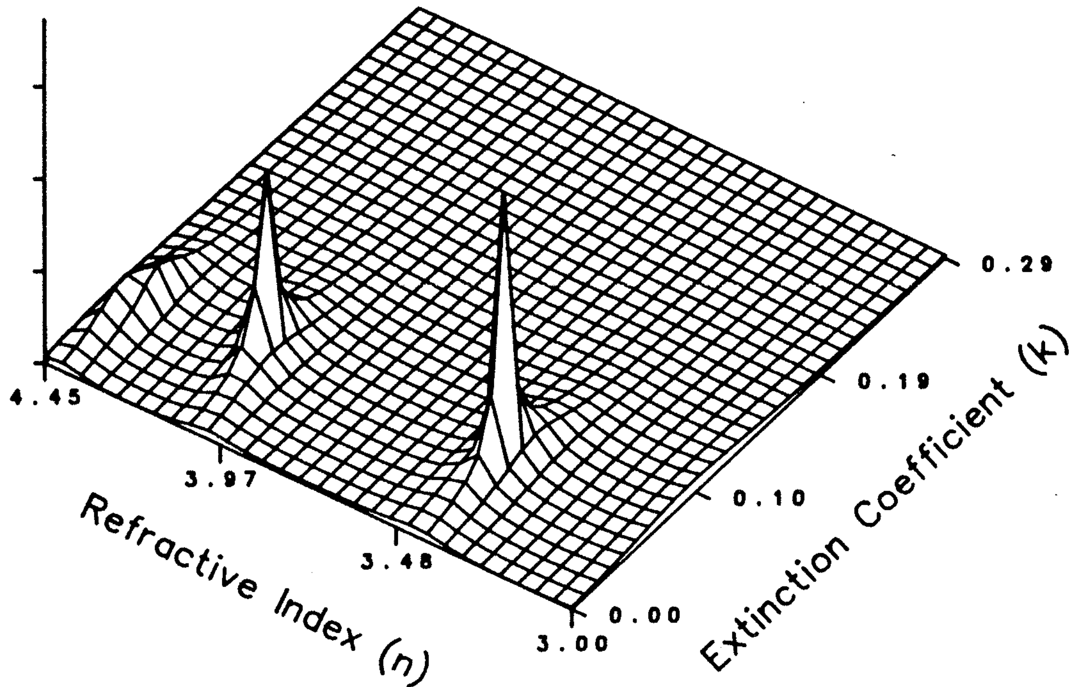

Figure 4.3: Inverse Error of Reflection and Transmission Coefficients. This plot is typical for the case of expected values of $R_0 = .332$ and $T_0 = .413$ where the determined values of n and k are 4.04 and 0.056 respectively.

Method Two

This method involves the measurement of the reflection coefficient and an approximate knowledge of the refractive index of the film.

Fig. 4.4 illustrates the peaks in reflectivity for a range of n and thickness values. From this figure it is

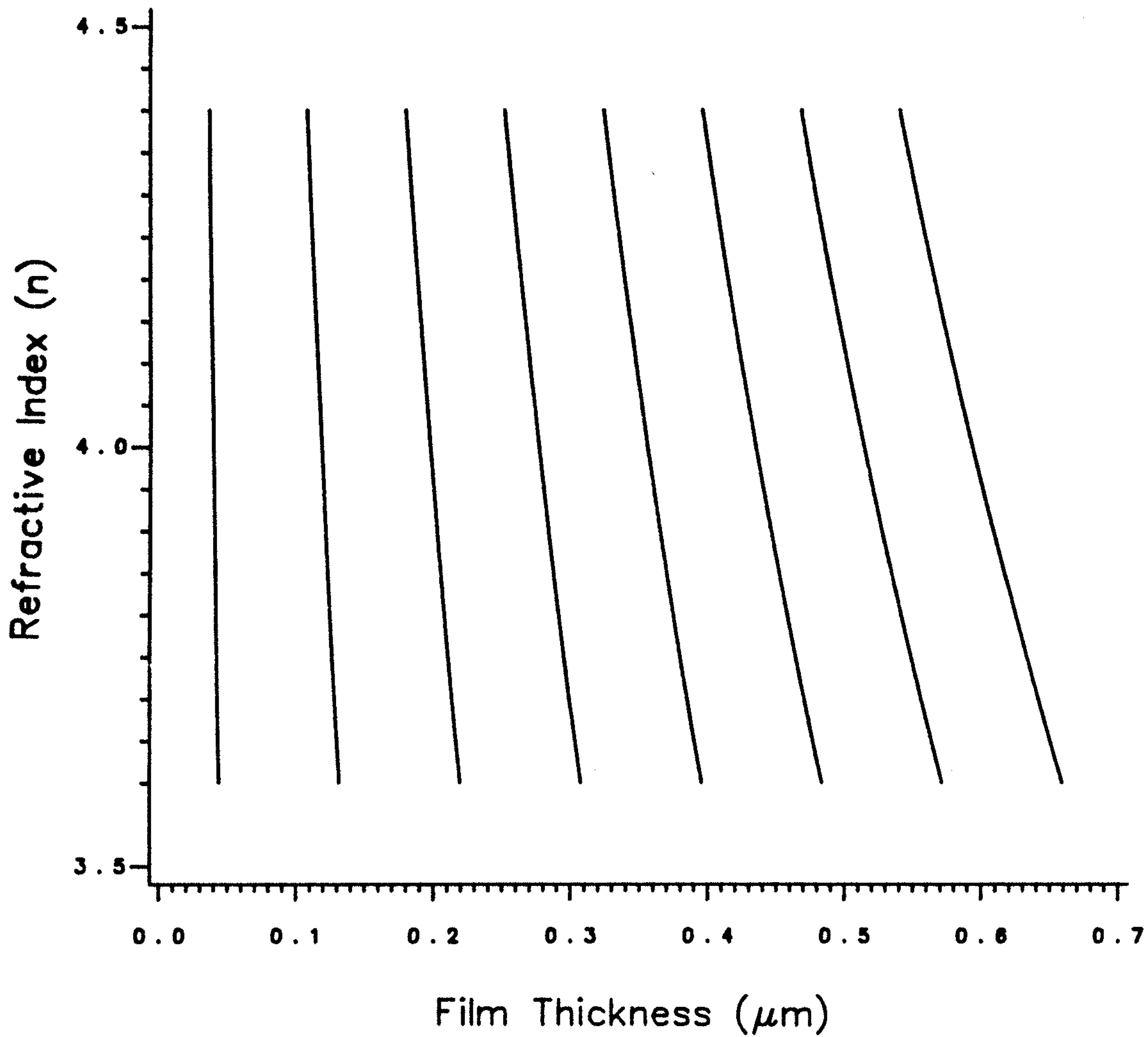

Figure 4.4: Peaks in Reflectivity as a Function of n and d

noted that the positioning of the peaks is not critical to the determination of the thickness when the thickness is small (< 0.5 μm). The thickness is determined as

$$d = \frac{\lambda}{4n}(1+2x), \qquad x = 0, 1, 2, \cdots \tag{4.2}$$

where x is the number of peaks, when n is approximatly 4.0. Over this range of thickness, the upper envelope of the reflection coefficient vs. thickness curve, shown in Fig. 4.5, can be modelled as

$$R = R_0 e^{-\beta d} \tag{4.3}$$

The envelope of the oscillations in Fig. 4.5 (peak-to-peak height vs thickness) does not obey a simple exponential dependence. However, the upper envelope alone (peaks for constructive interference) do closely approximate an exponential relation over a wide range of d. In fact, over a wide range of optical thicknesses (actually of the nd product), the value of β is approximately equal to the absorption coefficient. This is seen by Fig. 4.6 where the value of β vs α is plotted. As a result, it is evident that for the region of interest, we can model the upper envelope by the approximation

$$R = R_0 e^{-\alpha d} = R_0 e^{\frac{-4\pi k d}{\lambda}} \tag{4.4}$$

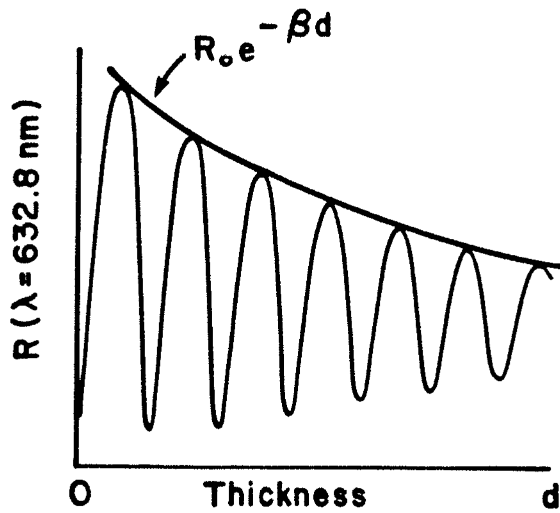

Figure 4.5: Upper Envelope of Reflection Curve

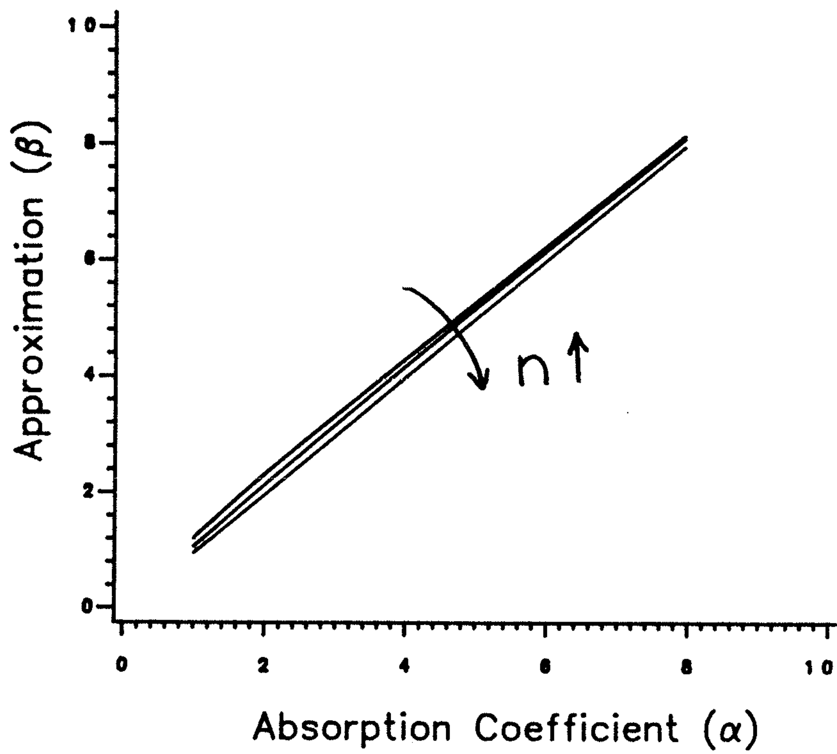

Figure 4.6: Envelope Decay β as a Function of α

4.1.4 Discussion

For convenience in process monitoring, the dependence of β, i.e. of the absorption coefficient α ,upon H content is given in Fig. 4.7. The dependence of upon H content is based upon measurements of a-Si:H films prepared by various techniques, and also deduced from optical absorption coefficients reported in the literature. The error bars represent the 95% confidence interval. In our studies, the hydrogen content was determined directly from infrared absorption studies, but these were not always the methods used in the experiments reported in the literature.

In view of the simplicity and non-invasive nature of reflectivity measurements at 632.8 nm with inexpensive HeNe laser sources, the present technique provides a direct method for routine in-situ analysis of H incorporation into the a-Si:H films during film growth. Process monitoring devices based upon these principles could also be constructed of solid-state lasers and photodiodes enclosed in a container with a window made of a suitable material. Such devices may be employed at many locations within the deposition chamber, thereby assisting in film quality-control. The film deposited on the container window would be subsequently removed with an etchant, enabling the device to be reused. These results are insensitive to other details of the fabrication procedure, and are expected to aid in the optimization of a-Si:H based devices.

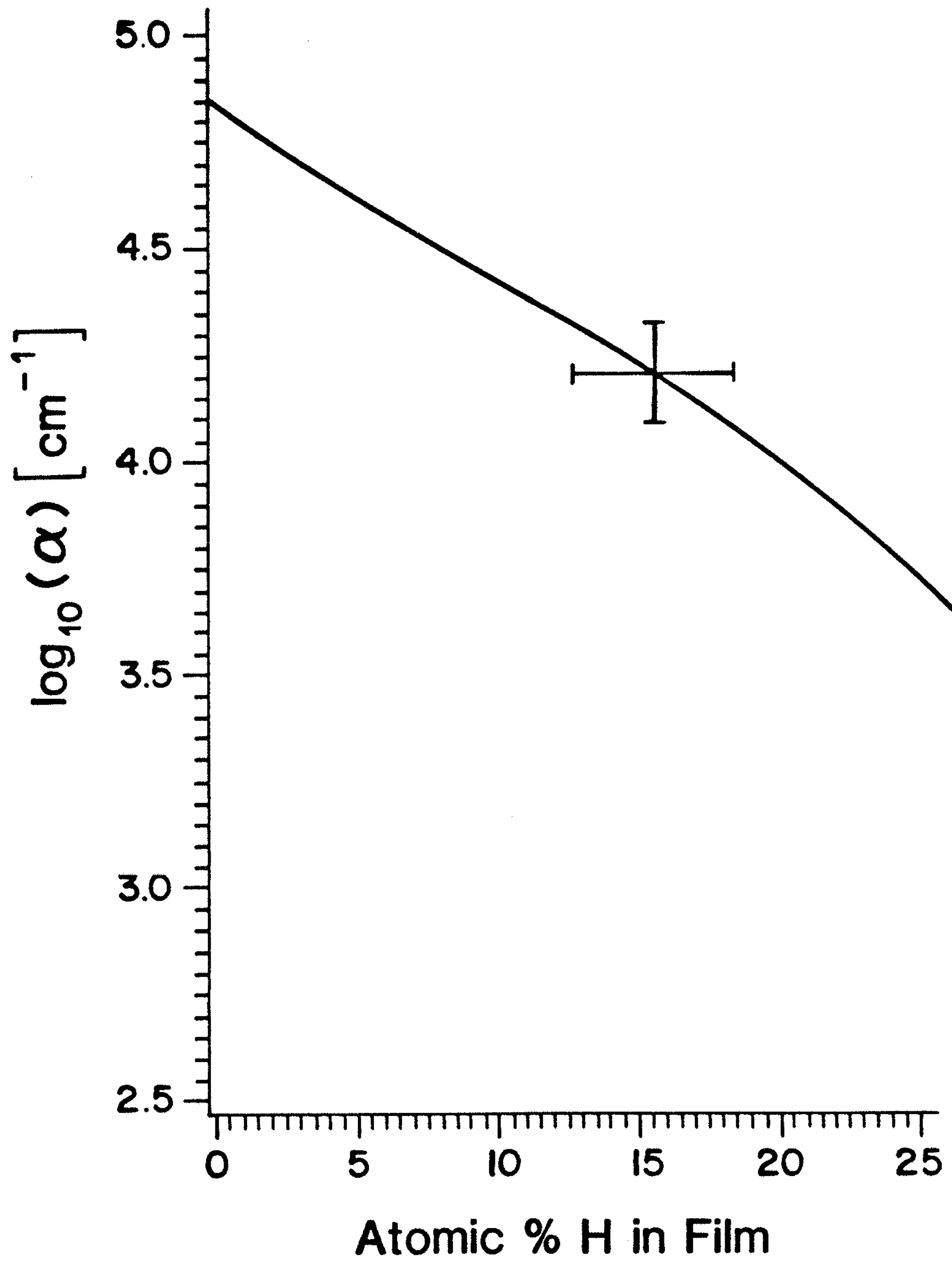

Figure 4.7: Absorption Coefficient (α) vs Hydrogen Content

Chapter V

CONCLUSIONS

Hydrogenated amorphous silicon has been fabricated for the first time by activated reactive evaporation. The electrical and optical properties of these films have been characterized and the results lead to the following conclusions:

1. High deposition rates with excellent film uniformity can be attained independent of the probe voltage. Typical deposition rates were 0.04 - 0.1 μm/min.
2. Dark conductivities and activation energies comparable to r.f. glow-discharge-produced films are possible with high hydrogen partial pressures and high activation voltages.
3. The increase in the long-wavelength refractive index for high activation voltages and large hydrogen partial pressures indicates the effectiveness of the method in achieving the incorporation of atomic hydrogen. This result is also confirmed by the increase in the optical gap for large hydrogen partial pressures.
4. The morphology of the films has been confirmed as amorphous, by Raman spectroscopy studies.

As a result of this work, it appears that the use of the ARE technique for a-Si:H fabrication is promising. The use of this method has many advantages that have yet to be demonstrated. These include the fabrication of hydrogenated and nitrogenated silicides and alloys in multiple gun evaporation systems.

The release of hydrogen from the a-Si:H network as a writing mechanism for archival storage has been proposed. The storage technique is based on the changes in reflectivity and conductivity for laser and electron-beam addressed systems. Based on experimental results on the evolution of hydrogen, the following conclusions are derived:

1. The energy requirement for hydrogen evolution is lower than that for ablative film removal. This eases the power requirements for the writing tools and provides for more efficient film processing.
2. The primary limitation on the density of storage appears to be based on thermal constraints. Storage densities of the order of 10^9 bits/in^2 for optical recording and 10^{11} bits/in^2 for electron-beam recording are predicted. Hence, the use of electron beams to record and retrieve information promises to result in extremely dense data storage devices.
3. Very high SNRs are predicted for electron-beam processing techniques since more than 4 orders of

magnitude changes in conductivity have been realized experimentally.

Although the proposed writing techniques are presently in the laboratory research stage and much work must still be performed, it is believed that the predictions presented are valid and possible advances in ultra high density storage devices may be derived from the proposed writing techniques.

An in-situ monitoring technique for the determination of a-Si:H quality and film thickness has been developed. These monitoring techniques are based on the predictable dependence of the optical constants upon the atomic hydrogen content in a-Si:H. Due to the primary dependence of the extinction coefficient upon the hydrogen content and due to the validity of the theoretical optical model as demonstrated by experiment, it is believed that a reasonably accurate determination of the hydrogen content is possible. The incorporation of such a monitoring device into a small package utilitizing solid state lasers and detectors provides for a versatile monitoring technique suitable for most fabrication facilities. Although this work has emphasized the determination of the hydrogen content in a-Si:H, it is probable that the technique will be applicable to the fabrication of other types of materials.

Appendix A

OPTICAL PROPERTIES OF THIN FILMS

The derivation of the reflection and transmission coefficients as a function of wavelength (λ), thickness (d), refractive index (n) and extinction coefficient (k) is presented. The solutions are derived for both the frontside and backside reflectivity as illustrated by the model used in Fig. 1 (a) and (b). Reflections at all interfaces, multiple reflections within the film and optical absorption are considered explicitly.

The derivation of the reflection and transmission coefficients are primarily a modified version of the two-film model presented by Heavens [56]. In this case, the quartz substrate is assumed to be semi-infinite in thickness and have a zero extinction coefficient. Derivations similar to Heavens have also been presented by Chopra [29], Denton et. al. [60] and Tomlin [61].

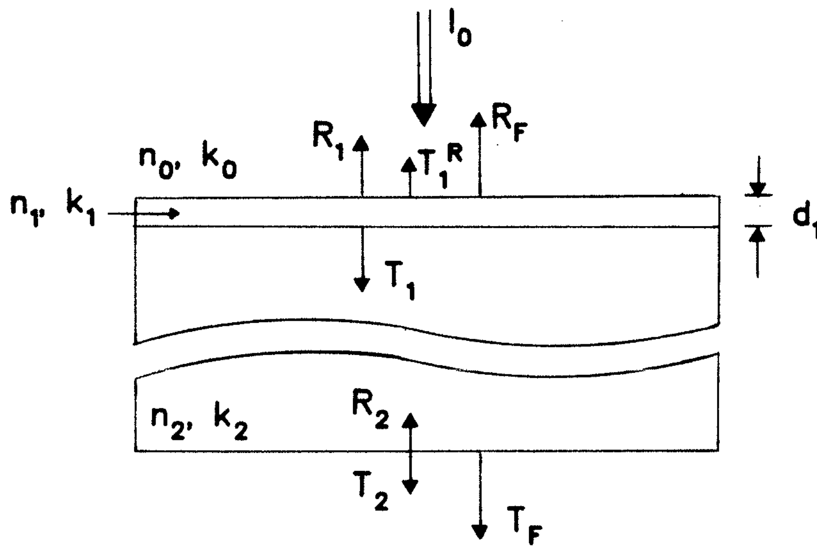

a) Frontside Illumination Model.

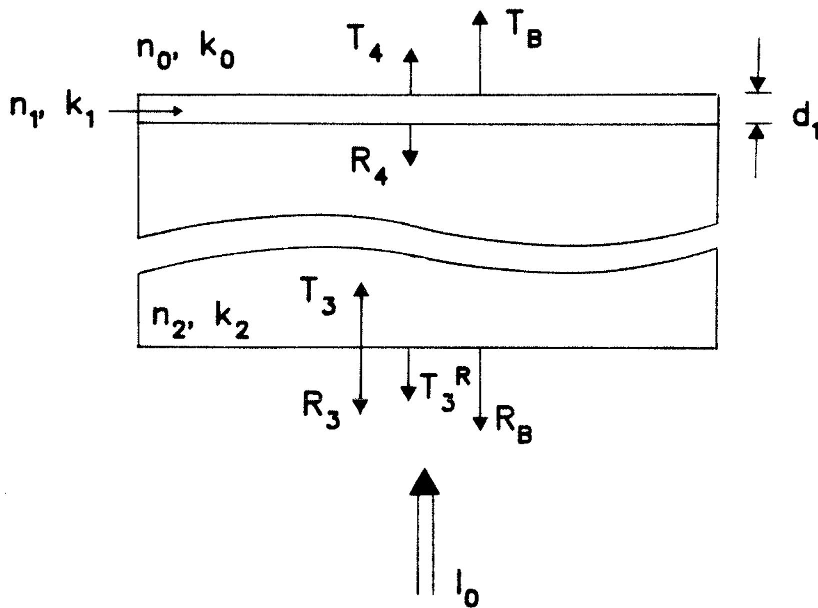

b) Backside Illumination Model.

Figure A.1: Thin Film Reflection and Transmission Models

At the film-air interface, for frontside illumination (Fig. A.1(a)), the reflection and transmission coefficient (R_1 and T_1) are calculated as follows:

Defining

n = refractive index of free space
n = refractive index of the thin films
k = extinction coefficient of the thin films
d = thin film thickness
n = refractive index of the quartz
λ = illumination wavelength

we have that

$$g_1 = \frac{n_0^2 - n_1^2 - k_1^2}{(n_0+n_1)^2+k_1^2} \qquad g_2 = \frac{n_1^2 - n_2^2 + k_1^2}{(n_1+n_2)^2+k_1^2}$$

$$h_1 = \frac{2n_0k_1}{(n_0+n_1)^2+k_1^2} \qquad h_2 = \frac{-2n_2k_1}{(n_1+n_2)^2+k_1^2}$$

$$\alpha_1 = 2\pi k_1 d_1/\lambda \qquad \gamma_1 = 2\pi n_1 d_1/\lambda$$

$$p_2 = e^{\alpha_1}\cos(\gamma_1)$$

$$q_2 = e^{\alpha_1}\sin(\gamma_1)$$

$$t_2 = e^{-\alpha_1}(g_2\cos(\gamma_1)+h_2\sin(\gamma_1))$$

$$u_2 = e^{-\alpha_1}(h_2\cos(\gamma_1)-g_2\sin(\gamma_1))$$

$$p_{12} = p_2+g_1t_2-h_1u_2$$

$$q_{12} = q_2+h_1t_2+g_1u_2$$

$$t_{12} = t_2+g_1p_2-h_1q_2$$

$$u_{12} = u_2+h_1p_2+g_1q_2$$

$$R_1 = \frac{t_{12}^2+u_{12}^2}{p_{12}^2+q_{12}^2} \tag{A.1}$$

$$T_1 = \frac{n_2}{n_0}\frac{[(1+g_1)^2+h_1^2][(1+g_2)^2+h_2^2]}{A+B+C+D} \tag{A.2}$$

where

$$A = e^{2\alpha_1}$$

$$B = (g_1^2+h_1^2)(g_2^2+h_2^2)e^{-2\alpha_1}$$

$$C = 2(g_1g_2-h_1h_2)\cos(2\gamma_1)$$

$$D = 2(g_1h_2-g_2h_1)\sin(2\gamma_1)$$

At the quartz-air interface, the reflection and transmission coefficients (R_2 and T_2) are calculated as :

$$R_2 = \frac{(n_2-n_0)^2}{(n_2+n_0)^2} \tag{A.3}$$

$$T_2 = \frac{4n_2n_0}{(n_2+n_0)^2} \tag{A.4}$$

In the quartz substrate, multiple reflections are not considered since it is assumed to be semi-infinite and the reflection coefficient R_2 is in any case very small. Therefore, the transmission value T_1^R is calculated with the following relation:

$$T_1^R(n_0,n_1,k_1,d_1,n_2,\lambda) = T_1(n_2,n_1,k_1,d_1,n_0,\lambda) \tag{A.5}$$

The resulting total reflection and transmission values (R_F and T_F) can then be calculated as:

$$R_F = R_1+T_1R_2T_1^R \tag{A.6}$$

$$T_F = T_1T_2 \tag{A.7}$$

For the case of in-situ film growth monitoring, as described in Chapter 4, illumination for the reverse (back) side is desirable (as in Fig. A.1(b)). Using the following relations

$$R_4(n_0,n_1,k_1,d_1,n_2,\lambda) = R_1(n_2,n_1,k_1,d_1,n_0,\lambda) \qquad \text{(A.8)}$$

$$T_4(n_0,n_1,k_1,d_1,n_2,\lambda) = T_1(n_2,n_1,k_1,d_1,n_0,\lambda) \qquad \text{(A.9)}$$

$$R_3 = R_2 \qquad \text{(A.10)}$$

$$T_3 = T_3^R = T_2 \qquad \text{(A.11)}$$

the values of R_B and T_B are calculated as

$$R_B = R_3 + T_3 R_4 T_3^R \qquad \text{(A.12)}$$

$$T_B = T_3 T_4 \qquad \text{(A.13)}$$

Examples of the reflection coefficients, as a function of thickness, using the values of

λ = 632.8 nm
n = 1.0
n = 4.0
k = 0.2
n = 1.5

are presented in Fig. A.2 and Fig. A.3 for the frontside and backside reflectivity respectively.

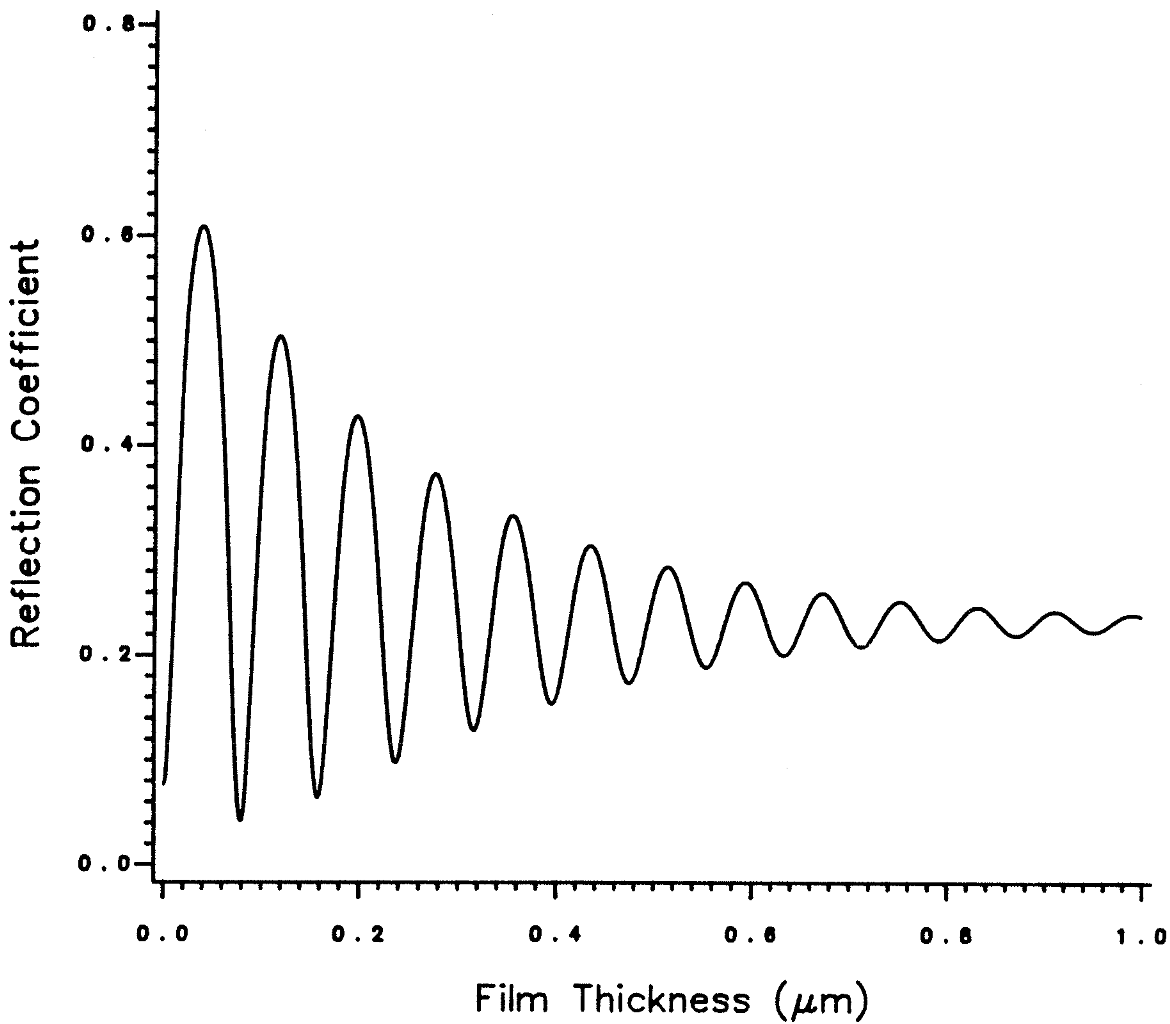

Figure A.2: Frontside Reflection Coefficient

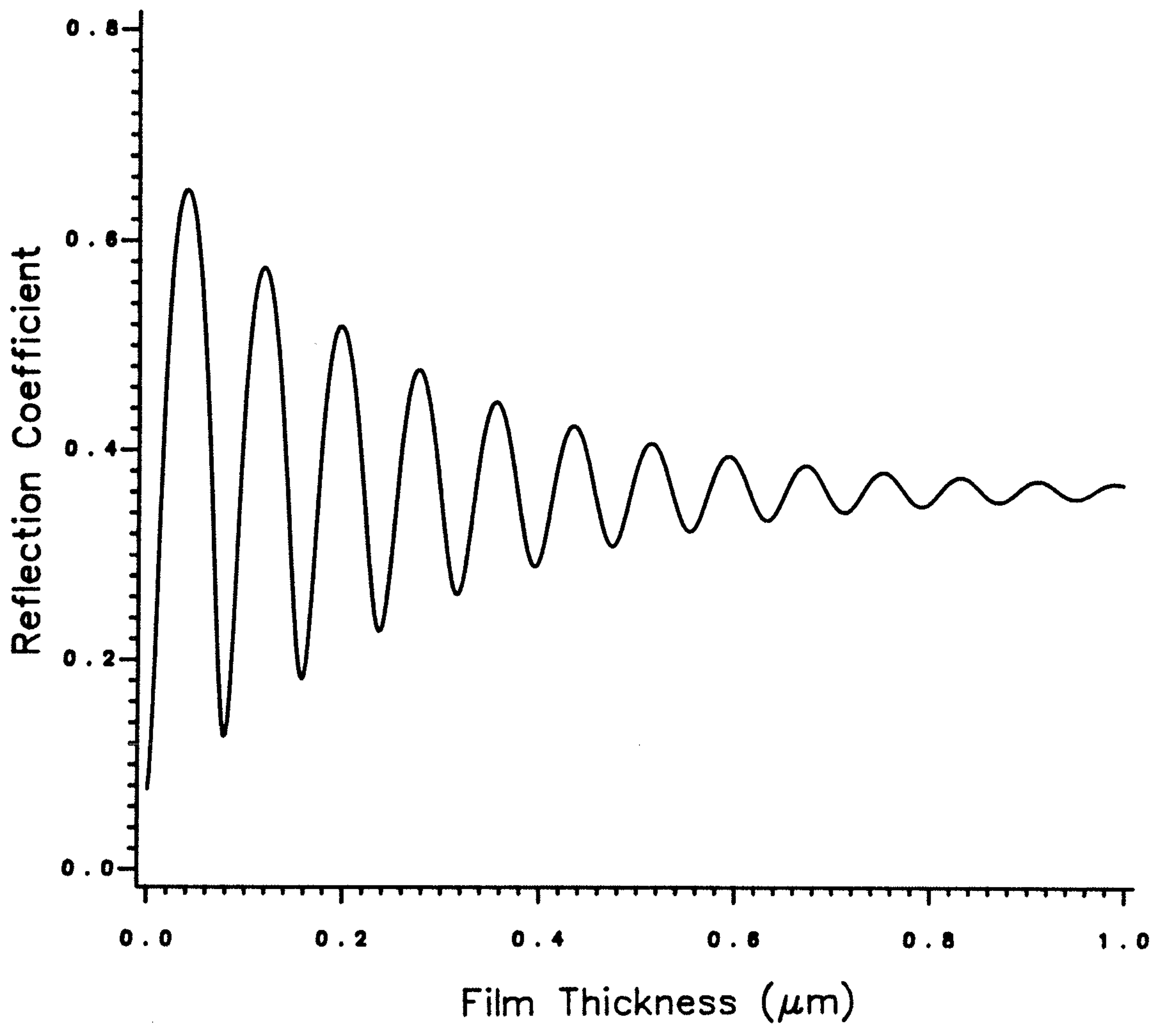

Figure A.3: Backside Reflection Coefficient

REFERENCES

1. W. Pries, R.D. McLeod, H.C. Card, K.C. Kao, "Properties of a-Si:H Deposited by Activated Reactive Evaporation", presented at the Materials Research Society Conference (Europe), Strassbourg, France. June 5-8, 1984.

2. R.D. McLeod, W. Pries, H.C. Card, K.C. Kao, "Hydrogenated Amorphous Silicon for Archival Storage", Applied Physics Lett., 1984, in press.

3. R.D. McLeod, W. Pries, H.C. Card, K.C. Kao, "Properties of a-Si:H for Optical Storage and Other Applications", to be published.

4. W. Pries, R.D. McLeod, H.C. Card, K.C. Kao, "A Mechanism for In-situ Monitoring of Hydrogen Incorporation into Amorphous Silicon", Applied Physics Lett., 1984, in press.

5. R.C. Chittick, J.H. Alexander, F.H. Sterling, "The Preparation and Properties of Amorphous Silicon", J. Electrochem. Soc., 116, pp. 77-81, 1969.

6. W.E. Spear, P.G. LeComber, "Investigation of the Localized State Distribution in Amorphous Si Films", J. Non-Cryst. Solids, 8-10, pp. 727-738, 1972.

7. A. Madan, P.G. LeComber, W.E. Spear, "Investigation of the Density of Localized States in a-Si using the Field Effect Technique", J. Non-Cryst. Solids, 20, pp. 239-257, 1976.

8. W.E. Spear, P.G. LeComber, "Substitutional Doping of Amorphous Silicon", Solid State Comm., 17, pp. 1193-1196, 1975.

9. W.E Spear, P.G. LeComber, "Electronic Properties of Substitutionally Doped Amorphous Si and Ge", Phil. Mag., 6, pp. 935-949, 1976.

10. W.E. Spear, P.G. LeComber, S. Kinmond, M.H. Brodsky, "Amorphous Silicon P-N Junction", Applied Physics Lett., 28, pp. 105-107, 1976.

11. D.E. Carlson, C.R. Wronski, "Amorphous Silicon Solar Cell", Applied Physics Lett., 28, pp. 671-673, 1976.

12. C.R. Wronski, D.E. Carlson, R.E. Daniel, "Schottky-Barrier Characteristics of Metal-Amorphous-Silicon Diodes", Applied Physics Lett., 29, pp. 602-605, 1976.

13. M. Matsumura, H. Hayama, Y. Nara, K. Ishibashi, "Amorphous Silicon Image Sensor IC", IEEE Electron Device Lett., 1, (9), pp. 182-184, 1980.

14. S. Kishida, Y. Nara, O. Kobayashi, M. Matsumura, "Amorphous-Silicon Charge-Coupled Devices", Applied Physics Lett., 41, pp. 1154-1156, 1982.

15. H. Adachi, K.C. Kao, "Dispersive Optical Constants of Amorphous Se_{1-x} Te_x Films", J. Applied Physics, 51, p. 6362, 1980.

16. I. Kato, H.C. Card, K.C. Kao, S.R. Mejia, L. Chow, "Microwave Sputtering System for the Fabrication of Thin Solid Films", Rev. Sci. Instrum., 53, p. 214, 1982.

17. S.R. Mejia, R.D. McLeod, K.C. Kao, H.C. Card, "The Effects of Deposition Parameters on a-Si:H Films Fabricated by Microwave Glow-Discharge Techniques", J. Non-Cryst. Solids, 59-60, pp. 727-730, 1983.

18. M.S. Mathur, H.C. Card, K.C. Kao, S.R. Mejia, G.C. Tabisz, "Far-Infrared Spectrum of a-Si:H Thin Films on Polyethylene", Can. J. Phys. 61, pp. 305-308, 1983.

19. K.C. Kao, R.D. McLeod, C.H. Leung, H.C. Card, H. Watanabe, "Dispersion of Optical Constants of Amorphous $Si_{1-x}Ge_x$ (H) Films Beyond Their Absorption Edges", J.Phys.D: Appl. Phys., 16, pp. 1801-1811, 1983.

20. R.D. McLeod, H.C. Card, K.C. Kao, H. Watanabe, "Optical and Electrical Properties of Amorphous Hydrogenated Si_{1-x} :Ge_x Thin Films", 1st Can. Conf. on Semiconductor Technology, Ottawa, Canada., 1983.

21. T.V. Herak, R.D. McLeod, K.C. Kao, H.C. Card, H. Watanabe, K. Katoh, M. Yasui, Y. Shibata, "Undoped Amorphous SiN_x :H Alloy Semiconductors: Dependence of Electronic Properties on Composition", J. Non-Cryst. Solids.

22. T.V. Herak, R.D. McLeod, M.G. Collet, K.C. Kao, H.C. Card, H. Watanabe, K. Katoh, M. Yasui, Y. Shibata, "Optical and Electronic Properties of Amorphous SiN_x :H Alloy Films", 2nd Can. Conf. on Semiconductor Technology, Ottawa, Canada., 1984.

23. S.R. Mejia, P.K. Shufflebotham, R.D. McLeod, W. Pries, K.C. Kao, H.C. Card, "Dynamic Laser Metalization for VLSI Interconnection", submitted to the IEDM 1984 Conf., San Fransisco, USA.

24. H. Okamoto, T. Yamaguchi, Y. Nitta, Y. Hamakawa, "Effect of DC Electric Field on the Basic Properties of RF Plasma Deposited a-Si", J. Non-Cryst. Solids, 35-36, pp. 201-206, 1979.

25. M. Taniguchi, M. Hirose, Y. Osaka, "Amorphous Silicon Hydrogen Alloys Produced under Magnetic Field", J. Non-Cryst. Solids, 35-36, pp. 189-194, 1979.

26. A.G. Dias, L. Guimaraes, R. Martins, "The Effect of Static Electric and Magnetic Fields on the Optical Properties of Amorphous Hydrogenated Silicon Films Produced by R.F. Glow Discharge", Thin Solid Films, 89, pp. 307-313, 1982.

27. N.F. Mott and E.A. Davis, Electronic Processes in Non-Crystalline Materials, Second Edition (Clarendon, Oxford, 1979).

28. S.R. Mejia, The Effects of Deposition Parameters on "Hydrogenated Amorphous Silicon Films Fabricated by Microwave Glow Discharge Techniques", M.Sc. Thesis Dissertation, University of Manitoba, 1984.

29. K.L. Chopra, Thin Film Phenomena, McGraw Hill, New York, 1969.

30. L. Kubler, J.J. Koulmann. R. Haug, A. Jaegle, "Evaporated a-Si Films with Low ESR Defect Density by Hydrogenation Under NH_3 Ambient", Solid State Comm., 48, (1), pp. 61-64, 1983.

31. L. Kubler, J.J. Koulmann. R. Haug, A. Jaegle, "Substrate Bias Effects on the Properties of Evaporated Amorphous Silicon Based Films", presented at the Materials Research Society Conference (Europe), Strassbourg, France. June 5-8, 1984.

32. V. Grasso, A.M. Mezzasalma, F. Neri, "A New Evaporation Method for Preparing Hydrogenated Amorphous Silicon Films", Solid State Comm., 41, (9), pp. 675-677, 1982.

33. M. Shindo, S. Sato, I. Myokan, S. Mano, T. Shibata, "Preparation and Analysis of Reactively Evaporated a-Si:H", J. Non-Cryst. Solids, 59-60, pp. 747-750, 1983.

34. J. Ishikawa, I.H. Wilson, "The Effects of Oxygen, Hydrogen, and Fluorine on the Conductivity of High Purity Evaporated Amorphous Silicon Films", J. Non-Cryst. Solids, 45, pp. 271-281, 1981.

35. J.I. Pankove, M.A. Lampert, M.L. Tarng, "Hydrogenation and Dehydrogenation of Amorphous and Crystalline Silicon", Applied Physics Lett., 32, pp. 439-441, 1978.

36. D. Kaplan, N. Sol, G. Velasco, P.A. Thomas, "Hydrogenation of Evaporated Amorphous Silicon Films by Plasma Treatment", Applied Physics Lett., 33, pp. 440-442, 1978.

37. A.C. Raghuram, R.F. Bunshah, "The Effect of Substrate Temperature on the Structure of Titanium Carbide Deposited by Activated Reactive Evaporation", J. Vac. Sci. Technol., 9, (6), pp. 1389-1394, 1972.

38. R.F. Bunshah, A.C. Raghuram, "Activated Reactive Evaporation Process for High Rate Deposition of Compounds", J. Vac. Sci. Technol., 9, (6), pp. 1385-1388, 1972.

39. P.J. Martin, R.P. Netterfield, W.G. Sainty, "Optical Properties of TiN_x Produced by Reactive Evaporation and Reactive Ion-beam Sputtering", Vacuum, 32, (6), pp. 359-362, 1982.

40. M.H. Brodsky, R.S. Title, K. Weiser, G.D. Pettit, "Structural, Optical and Electrical Properties of Amorphous Silicon Films", Phys. Rev. B, 1, pp. 2632-2641, 1970.

41. R. Schwidefsky, "Increase of the Refractive Index of Silicon Films by Dangling Bonds", Thin Solid Films, 18, pp. 45-52, 1973.

42. M.H. Brodsky, "Quantum Well Model of Hydrogenated Amorphous Silicon", Solid State Comm., 36, pp. 55-59, 1980.

43. N. Kniffler, B. Schroeder, J. Geiger, "Vibrational Spectroscopy of Hydrogenated Evaporated Amorphous Silicon Films", J. Non-Cryst. Solids, 58, pp. 153-163, 1983.

44. G.C. Kenney, D.Y.K. Lou, R. McFarlane, A.Y. Chan, J.S. Nadan, T.R. Kohler, J.G. Wagner, F. Zernike, "An Optical Disk Replaces 25 Mag Tapes", IEEE Spectrum, 16, (2), pp. 33-38, 1979.

45. V.B. Jipson, K.Y. Ahn, "Materials for Optical Storage", Solid State Tech., pp. 141-146, Jan. 1984.

46. J. Gosch, "Mass Tape Memory Holds 600 Gigabytes with 10-s Access", Electronics, 57, (7), pp. 73-74, 1984.

47. H.R. Shanks, L. Ley, "Formation of Pin Holes in Hydrogenated Amorphous Silicon at High Temperatures and the Yield Strength of a-Si:H", J. Applied Physics, 52, pp. 811-813, 1981.

48. M. Janai, F. Moser, "Optical Recording in Amorphous Silicon Films", J. Applied Physics, 53, pp. 1385-1386, 1982.

49. P. John, B.L. Jones, "Optical Recording in Hydrogenated Amorphous Silicon", Applied Physics Lett., 45, pp. 39-41, 1984.

50. A.B. El-Kareh, K.Y. Morovan, M.A. Smither, "Temperature Profiles of Targets Bombarded by Electron Beams", J. Applied Physics, 48, pp. 2356-2359, 1977.

51. M.A. Bosch, "Optical Recording in Hydrogenated Semiconductors", Applied Physics Lett., 40, pp. 8-10, 1982.

52. H. Fritzsche, C.C. Tsai, P. Persans, "Amorphous Semiconducting Silicon-Hydrogen Alloys", Solid State Tech., 21, pp. 55-60, 1978.

53. N. Fukada, T. Imura, A. Hiraki, T. Itahashi, T. Fukada, M. Tanaka, "Sensitive Detection of Hydrogen in a-Si:H by Coincidence Measurement of Elastically Scattered 100 MeV $^3He^{2+}$ Ions and Recoil Protons", Jap. J. Applied Physics (Lett.), 21, p. 532, 1983.

54. W. Beyer, H. Wagner, "The Role of Hydrogen in a-Si:H - Results of Evolution and Annealing Studies", J. Non-Cryst. Solids, 59-60, pp. 161-168, 1983.

55. E.C. Freeman, W. Paul, "Optical Constants of RF Sputtered Hydrogenated Amorphous Si", Phys. Rev. B, 20, pp. 716-728, 1979.

56. O.S. Heavens, Optical Properties of Thin Solid Films, Dover Press, pp. 74-78, 1965.

57. M. Lax, "Temperature Rise Induced by a Laser Beam", J. Applied Physics, 48, pp. 3919-3924, 1977.

58. S. Schiller, U. Heisig, S. Panzer, Electron Beam Technology, John Wiley, New York, 1982.

59. J.A. McMillan, E.M. Peterson, "Kinetics of Decomposition of Amorphous Hydrogenated Silicon Films", J. Applied Physics, 50, pp. 5238-5241, 1979.

60. R.E. Denton, R.D. Campbell, S.G. Tomlin, "The Determination of the Optical Consants of Thin Films from Measurements of Reflectance and Transmitance at Normal Incidence", Applied Physics, 5, pp. 852-863, 1972.

61. S.G. Tomlin, "More Formulae Relating to Optical Reflection and Transmission by Thin Films", Applied Physics, 5, pp. 847-851, 1972.